Review Article

Recent advances in photonics of three-dimensional Dirac semimetal Cd$_3$As$_2$

Renlong Zhou,[a] Kaleem Ullah[ORCID],[b] Naveed Hussain,[c] Mohammed M. Fadhali[ORCID],[d,e] Sa Yang,[a] Qiawu Lin,[a] Muhammad Zubair[ORCID],[f] and Muhammad Faisal Iqbal[ORCID][g,h,*]

[a]Guangdong University of Education, School of Physics and Information Engineering, Guangzhou, China
[b]University of Delaware, Department of Electrical and Computer Engineering, Newark, Delaware, United States
[c]University of California, Department of Electrical Engineering and Computer Science, Irvine, California, United States
[d]Jazan University, Faculty of Science, Department of Physics, Jazan, Saudi Arabia
[e]Ibb University, Faculty of Science, Department of Physics, Ibb, Yemen
[f]Institute of Energy and Climate Research, Materials Synthesis and Processing (IEK-1), Forschungszentrum Jülich GmbH, Jülich, Germany
[g]University of Science and Technology of China, Hefei National Laboratory for Physical Sciences at the Microscale, Hefei, China
[h]Riphah International University Faisalabad, Department of Physics, Faisalabad, Pakistan

Abstract. Due to their unusual features in condensed matter physics and their applicability in optical and optoelectronic applications, three-dimensional Dirac semimetals (3D DSMs) have garnered substantial interest in recent years. In contrast to monolayer graphene, 3D DSM exhibits linear band dispersion despite its macroscopic thickness. Therefore, being a bulk material, it is easy to make nanostructures with 3D DSM, just as one normally does with metals such as gold and silver. Among 3D DSMs, cadmium arsenide (Cd$_3$As$_2$) is quite famous and considered an excellent 3D DSM due to its chemical stability in air and extraordinary optical response. In this review, advances in 3D DSM Cd$_3$As$_2$ fabrication techniques and recent progress in the photonics of 3D DSM Cd$_3$As$_2$ are given and briefly reviewed. Various photonic features, including linear and nonlinear plasmonics, optical absorption, optical harmonic generation, and ultrafast dynamics, have been explored in detail. It is expected that Cd$_3$As$_2$ would share an excellent tunable photonic response like graphene. We envision that this article may serve as a concise overview of the recent progress of photonics in 3D DSM Cd$_3$As$_2$ and provides a compact reference for young researchers.

Keywords: Three-dimensional Dirac semimetal; Cd$_3$As$_2$; photonics; tunable; nanostructures.

1 Introduction

Traditionally, band theory classifies materials into insulators and metals based on whether a finite bandgap exists. It was recently discovered that insulators may be categorized further into normal and topological insulators based on the topology of their electronic structures.[1,2] Interestingly, there is an intermediary state between insulators and metals in which the conduction and valence bands meet only at discrete spots, resulting in a zero bandgap and singular points on the Fermi surface, of which graphene is a well-known example.[3] Graphene is a Dirac semimetal (DSM) with a linear band dispersion, in which massless Dirac

fermions imitate the low-energy states of relativistic particles.[4–8] Due to the high carrier velocity and the lack of backscattering, the mobilities of DSMs are exceptionally high, enabling novel applications in electronics and optoelectronics.[7,9–11] Early Dirac fermion realizations are restricted to two-dimensional (2D) systems. Recent Dirac system research has shifted its emphasis to the investigation of a unique quantum state of matter known as three-dimensional DSM (3D DSM).[3,12–15] As compared to 2D DSM, 3D DSM has comparable optoelectronic capabilities with the added benefit of stronger light–matter interactions due to its 3D structure.[16–18] The description of charge carriers in both 2D and 3D DSMs are governed by Dirac physics, hence, it is largely expected that 3D DSMs exhibit Dirac-type optical properties similar to graphene, such as tunable optical conductivity, high

*Address all correspondence to Muhammad Faisal Iqbal, iqbal@mail.ustc.edu.cn

nonlinear optical coefficients, and stronger light confinement.[19] In addition, the 3D structure of 3D DSM provides an extra degree of freedom, making it superior to 2D graphene for plasmonic waveguide construction.[16,19] Based on these remarkable characteristics, 3D DSM is an appropriate substitute for 2D DSM. For its exceptional features, 3D DSM has gained a lot of attention recently from many researchers. An external gate voltage may dynamically change the Fermi level and relative permittivity of 3D DSM, much like it does with graphene.[20,21] Additionally, because the crystalline symmetry is preserved in 3D DSM, a very high carrier mobility of 9×10^6 cm^2/(V.s) may be produced at 5 K, which is greater than that of graphene $[2 \times 10^5$ cm^2/(V.s)].[22]

The 3D DSM's unique electronic structure not only enables the study of numerous unusual phenomena, such as unusually high bulk carrier mobility,[23] high-temperature linear quantum magnetoresistance,[24,25] oscillating quantum spin Hall,[26] and giant diamagnetism,[27] but also serves as a platform for realizing various graphene applications in 3D materials. Additionally, unlike graphene, the 3D Dirac fermions in a 3D DSM are resistant to the spin-orbit interaction.[28] Apart from these remarkable features, when further symmetry is violated, 3D DSMs may be pushed into a variety of different quantum states, including the Weyl semimetal,[29] axion insulator,[30] and topological superconductor.[31] This adaptability enables the 3D DSM to be used for the fabrication of additional materials and the research of different topological quantum phase transitions. Recent exciting experiments have demonstrated the generation of terahertz radiation up to the third and seventh harmonics,[32] and a theoretical study predicted the generation of harmonics beyond the 31st order[33] with conversion efficiencies far exceeding those of graphene's high harmonic generation (HHG) due to finite interaction volume. As a result of these properties, 3D DSMs are appealing prospects for novel nanophotonic and nanoplasmonic applications as well as feasible substitutes for graphene. Cd₃As₂ is among the most stable 3D DSMs and has a huge linear energy-momentum space, which permits much experimental research.

In this review, we describe the state-of-the-art advances in the photonics of the 3D DSM Cd₃As₂. We will cover topics including optical harmonic generation (OHG), plasmonics, ultrafast dynamics, photonic modes, optical absorbers, and some others. In addition, a short review of recent advances in the fabrication procedures of Cd₃As₂ is presented. The first section of this review provides an overview of the 3D DSM, with an emphasis on Cd₃As₂ material. The theoretical foundations of photonics in 3D DSMs are presented in Sec. 2. In Sec. 3, several Cd₃As₂ fabrication strategies are presented. Section 4 discusses recent experimental and theoretical findings on a variety of photonics phenomena in 3D DSMs. Section 5 provides a short outline of the applications made possible by the photonics of Cd₃As₂. Finally, concluding remarks outline existing experimental and theoretical understandings as well as future research opportunities.

2 Theoretical Basis

A thorough knowledge of the fundamental material properties of 3D DSM (Cd₃As₂) has become critical for the right interpretation of a broad variety of observed and still unknown physical phenomena. Cd₃As₂ has a rather complicated crystal structure [Fig. 1(a)] with a unit cell containing 160 atoms. According to the current consensus, Cd₃As₂ is a tetragonal material with a unit cell of $a = b \approx 1.26$ nm and $c \approx 2.54$ nm at room and lower temperatures, which are the most important for basic and practical study of this material. The specific space group remains a point of contention. Recent research indicates that the centrosymmetric space group I4₁/acd (No. 142)[36,37] is preferable to the noncentrosymmetric space group I4₁cd (No. 110), as previously proposed.[38] For a complete understanding of Cd₃As₂, assigning the correct space group is of critical importance. The spin degeneracy is lifted when space inversion symmetry is absent, which may result in the Dirac nodes splitting into pairs of Weyl nodes.[36] A further point of interest is the fact that the crystal structure of Cd₃As₂, though clearly tetragonal, remains nearly cubic ($2a = 2b \approx c$).[34] Thus, the lattice may be thought of as a collection of antifluorite (cubic) cells devoid of two cadmium cations [Fig. 1(a)]. A relatively big unit cell of Cd₃As₂ is generated due to the cadmium vacancy ordering.

Additionally, it is necessary to emphasize that the crystal structure of Cd₃As₂ experiences a series of polymorphic phase changes above ambient temperature. Each of these phase transitions is followed by a sharp shift in the crystal's lattice constants, which may result in microcracks. Notably, regardless of the growth process, crystals of Cd₃As₂ can only be formed at temperatures more than 425°C. The intricacy of the crystal lattice has a direct effect on both the physical characteristics of Cd₃As₂ and our understanding of them. The electronic structure of Cd₃As₂ was investigated by many groups using angle-resolved photoemission spectroscopy (ARPES).[3,12,13,34] Cd₃As₂ possesses a pair of 3D Dirac fermions near the Γ point, with strong anisotropy between the k_z and k_x/k_y momentum directions detected through the analysis of the band dispersions along the k_x, k_y, and k_z momentum directions. With a comprehensive map of the 3D Brillouin zone, it is feasible to find the Dirac points and examine their dispersions along all three momentum directions (k_x, k_y, and k_z). The cone shape dispersion along the k_x and k_y directions can be seen in Fig. 1(e), where the 3D plot of the ARPES spectra intensity clearly demonstrates linear dispersions along both directions with limited anisotropy. Figure 1(d) illustrates that the contour plots at different binding energies exhibit a cone-shaped dispersion that becomes ring-shaped at higher binding energies, evolving from a point (the Dirac point).

A random phase approximation theory (RPA) can be used to calculate the complex conductivity of the DSM.[35] By incorporating the intraband and interband contributions to the dynamic conductivity of the DSM,[35] one can develop the following equation:

$$\operatorname{Re} \sigma(\Omega) = \frac{e^2}{\hbar} \frac{g}{24\pi} \Omega G\left(\frac{\pi}{2}\right), \tag{1}$$

$$\operatorname{Im} \sigma(\Omega) = \frac{e^2}{\hbar} \frac{g}{24\pi^2} \left\{ \frac{4}{\Omega} \left[1 + \frac{\pi^2}{3} \left(\frac{T}{E_F} \right)^2 \right] \right. \\ \left. + 8\Omega \int_o^{\varepsilon_c} \left[\frac{G(\varepsilon) - G(\Omega - 2)}{\Omega^2 - 4\varepsilon^2} \right] \varepsilon \mathrm{d}\varepsilon \right\}, \tag{2}$$

where $G(E) = n(-E) - n(E)$ with $n(E)$ being the Fermi distribution function, E_F is the Fermi level, $k_F = E_F/hv_F$ is the Fermi momentum with v_F equal to 10^6 m/s, $\varepsilon = E/E_F$, $\Omega = \hbar\omega/E_F$, $\varepsilon_c = E_c/E_F$ (E_c is the cutoff frequency), and g is the degeneracy factor. At low-temperature limit $T \ll E_F$, the Eqs. (1) and (2) can be written as
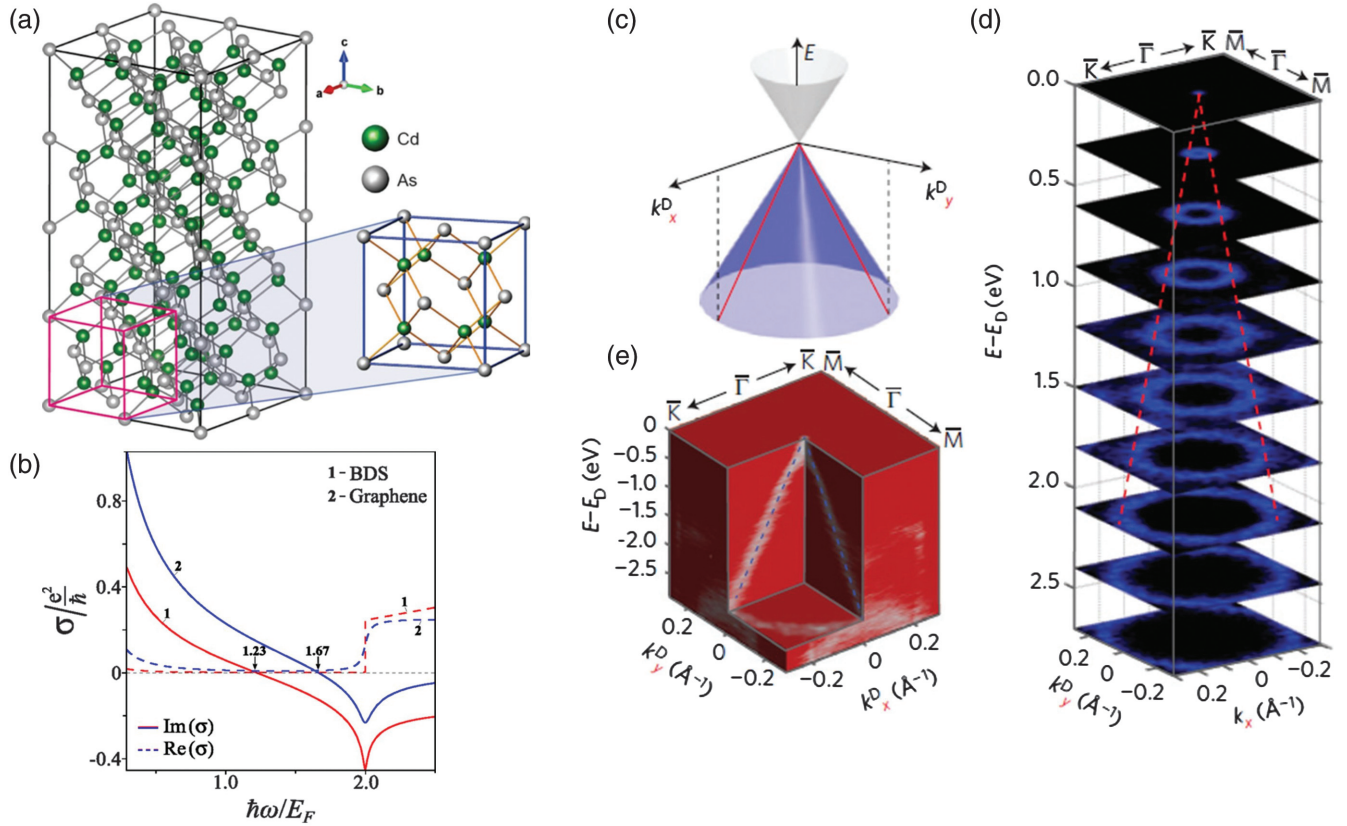
Fig. 1 Crystal structure, projections of the 3D Dirac fermions, and refractive index of 3D DSM. (a) Cd_3As_2's nonprimitive tetragonal unit cell is made up of 24 slightly deformed antifluorite cells with two cadmium vacancies. 96 cadmium atoms and 64 arsenic atoms are contained in this cell. (b) The real and imaginary components of dynamic conductivity in 3D DSMs. (c) Schematic representation of the projected Dirac cone into the (k_x, k_y, E) space reconstructed from experimental values. The red lines show the linear dispersions along the k_x and k_y axes. (d) Stacking plots of constant-energy contours at different binding energies reveal the structure of the Dirac cone band. The red dotted lines serve as visual cues for the dispersions and intersect at the Dirac point. (e) A three-dimensional intensity plot of the photoemission spectrum at the Dirac point, demonstrating identical cone-shaped dispersion to that in (c). The figure is reproduced with the permission of (a) Ref. 34 © 2018 American Physical Society, (b) Ref. 35 © 2016 American Physical Society, and (c)–(e) Ref. 3 © 2018 Nature Publishing Group.

$$\text{Re } \sigma(\Omega) = \frac{e^2}{\hbar} \frac{g}{24\pi} \Omega \theta(\Omega - 2), \tag{3}$$

$$\text{Im } \sigma(\Omega) = \frac{e^2}{\hbar} \frac{g}{24\pi^2} \left[\frac{4}{\Omega} - \Omega \ln\left(\frac{4\varepsilon_c^2}{|\Omega^2 - 4|} \right) \right]. \tag{4}$$

In Eq. (4), the first term comes from the intraband conductivity and has a Drude-like form. On the other hand, the second logarithmic term represents the negative contribution of the interband transitions (the dielectric response). As demonstrated in Eq. (3), the real component of the 3D DSM conductivity is likewise derived from interband transitions and is responsible for optical absorption. Unlike graphene, which exhibits constant absorption, 3D DSM has a linear frequency absorption, as empirically demonstrated.[39–41] It is evident from Eq. (4) that the imaginary part of 3D DSM conductivity differs from graphene due to its cutoff energy dependence. It should be noted,

however, that in 3D DSM, the dielectric response is dominant at some frequencies. Further, in 3D DSM, the dielectric response may be observed at frequencies below Ω_0 because of the interband contributions from bands lower than the valence one that are not taken into account in Eqs. (3) and (4). Thus, in order to conduct an effective analysis of the dielectric response, one must investigate the dielectric function of 3D DSM in depth.

3 Fabrication Techniques

Cd_3As_2 growing technology comprises a variety of techniques stretching back over fifty years. These provide a variety of sample morphologies, including bulk or needle-like crystals, thin films, microplatelets, and nanowires. In addition to mono-crystalline and poly-crystalline samples, there are also amorphous samples with varying qualities and doping levels. The high carrier density (from 4.4×10^{18} to 1.5×10^{19} cm^{-3}) of Cd_3As_2 in bulk pushes the Fermi level further from the Dirac point.[42] This high carrier density can be suppressed by reducing the

dimensions of Cd_3As_2 from bulk to thin films and nano-structures.[43] In addition, Cd_3As_2 displayed good optoelectronic capabilities and high energy conversion properties that rely largely and significantly on the synthesis methodologies.[44] To achieve excellent device performance, the synthesized Cd_3As_2 thin films and nanostructures must have excellent crystalline quality and unique morphologies. In recent years, there has been considerable interest in the development and characterization of Cd_3As_2. The thin films and nanostructures of Cd_3As_2 can be synthesized by various methodologies, namely, physical vapor deposition (PVD),[44] pulse laser deposition (PLD),[45] molecular beam epitaxy (MBE),[46] chemical vapor deposition (CVD),[47] and self-selecting vapor growth (SSVG).[34] In this section, a quick overview of the specifics of these synthesis procedures will be provided.

3.1 Molecular Beam Epitaxy

MBE is a robust deposition method for the development of high-quality, large-area epitaxial thin films. MBE is better than CVD and other deposition techniques due to its capacity to build heterostructures and superlattices with abrupt interfaces, as well as its chemical component versatility and fine control over film thickness. The ultrahigh vacuum (up to 10^{-10} mbar) in the MBE work chamber causes the formation of very pure thin films. In addition, several characterization techniques including ARPES and reflection high-energy electron diffraction (RHEED), can be coupled with MBE to *in situ* monitor the deposition process and electronic structure.[48] Based on these outstanding features, MBE is a highly suitable deposition technique to grow Cd_3As_2 thin films and their heterostructures. Liu et al.[21] reported the first-ever growth of Cd_3As_2 thin films by using the MBE technique and they demonstrated tunable properties like ambipolar effect and quantum oscillations in deposited wafer-scale films. The combined MBE and PLD technique was employed by Uchida et al.[45] to achieve Cd_3As_2 thin films with high-crystallinity and high-mobility. Schumann et al.[49] used MBE to create highly crystalline epitaxial Cd_3As_2 thin films. They discovered an expanded energy gap in bulk electronic states and, at low temperatures, the adequate mobility of carriers in surface states made it possible to investigate quantized Hall effects in MBE-grown Cd_3As_2 thin films. Yang et al.[46] fabricated Cd_3As_2/organic thin film p–n heterojunction-based ultraviolet (UV) to long-wave infrared (LIR) photodetectors via MBE. The MBE grown heterostructures-based device showed excellent responsivity of 729 mA/W, fast response time higher than 282 μs, and a high on–off ratio of 6268. In LIR region, the responsivity and on–off ratios were 81.3 mA/W and 100, respectively.[46] As demonstrated in Fig. 2(c), these Cd_3As_2/organic thin film photodetectors are very flexible. The findings revealed that Cd_3As_2/organic thin film p–n heterojunction devices generated by MBE are highly desirable for high-speed and wide-band photodetectors.

3.2 Pulse Laser Deposition

PLD is a very advantageous process for depositing thin films of materials with high melting points, complicated stoichiometry, and sandwich architectures. In PLD the source material is bombarded with a high-energy focused pulsed laser and the small bombarded region converts into a plasma state. This bombarded pulse can raise the temperature of that microregion up to ten thousand degrees in no time. Since the high energy source is located outside the working chamber, PLD provides

the flexibility of deposition in both ultrahigh vacuum (UHV) and inert gas environments. In UHV, the particles have eccess energy resulting in the deposition of nanocrystalline supersaturated solid solution and amorphous alloys. In the ambient inert gas environment, the energy of the particles can be controlled; consequently, the properties of deposited films can be tuned. The most important feature of PLD is to grow highly stoichiometric thin films of various kinds of materials ranging from metals to semiconductors and insulators. The thin film deposition rates of PLD are high as compared with other deposition techniques and multilayered structures can be grown easily.[54,55] These attributes make PLD a highly desirable technique to grow thin films of 3D DSM Cd_3As_2. As illustrated in Fig. 2(d), Dubowski and colleagues[51] used the PLD approach to develop stoichiometric polycrystalline Cd_3As_2 on quartz substrates at ambient temperature, which was 140 K lower than the temperature necessary to create equivalent films via thermal evaporation. The carrier concentration and mobility of PLD grown films were reported to be $(3.3-3.5) \times 10^{18}$ cm³ and $(0.6-1.0) \times 10^3$ cm² V^{-1} s^{-1}, respectively. To investigate the quantum transport phenomena in 3D DSM Cd_3As_2 requires a high-quality Cd_3As_2 film. Uchida et al.[45] established a growth approach by combining PLD and solid phase epitaxy to generate high-quality single-crystalline Cd_3As_2 films with controllable thickness, and they evaluated the influence of thickness on the quantum Hall effect. The quantum Hall states shown in high-quality Cd_3As_2 films open the way for quantum transport and device application research in topological DSM.

3.3 Physical Vapor Deposition

PVD encompasses a wide range of thin film deposition and nanostructure fabrication processes, including evaporation, sputtering, laser ablation deposition, vacuum arc-based deposition, and several more. In PVD, the atoms or clusters of atoms of solid materials are typically removed by either thermal heating the source material or bombarding it with very energetic particles such as electrons, atoms, molecules, ions, or photons.[48] In evaporation and ablation deposition, the removal process is thermodynamical. In sputtering, on the other hand, the removal of atoms from the source material is accomplished by a series of collisions with energetic particles at the material's surface, a process known as the kinetic ejection of atoms. These ejected species pass through an evacuated chamber and strike the substrate, forming thin films.[56] Li et al.[44] have successfully synthesized extremely crystalline Cd_3As_2 nanoplates and nano-octahedrons in a horizontal furnace using the PVD technique. Figure 2(a) depicts the nucleation and growth process of Cd_3As_2 nanostructures. The fabricated nanostructures/metal electrode exhibited good photovoltaic performance for self-powered photo-detection applications.

3.4 Chemical Vapor Deposition

Among all other deposition techniques, CVD provides feasibility to synthesize both thin films and nanostructures for large-area synthesis. In CVD, thin films or nanostructures are formed on heating substrates by means of a chemical reaction of gaseous or vapor species. This process can involve a variety of gaseous, liquid, and solid chemicals as source material for the fabrication of thin films. As compared to other deposition techniques, CVD is more versatile, adaptable, compatible, simplest, reproducible, productive, and cost-effective.[52,57,58] All of these
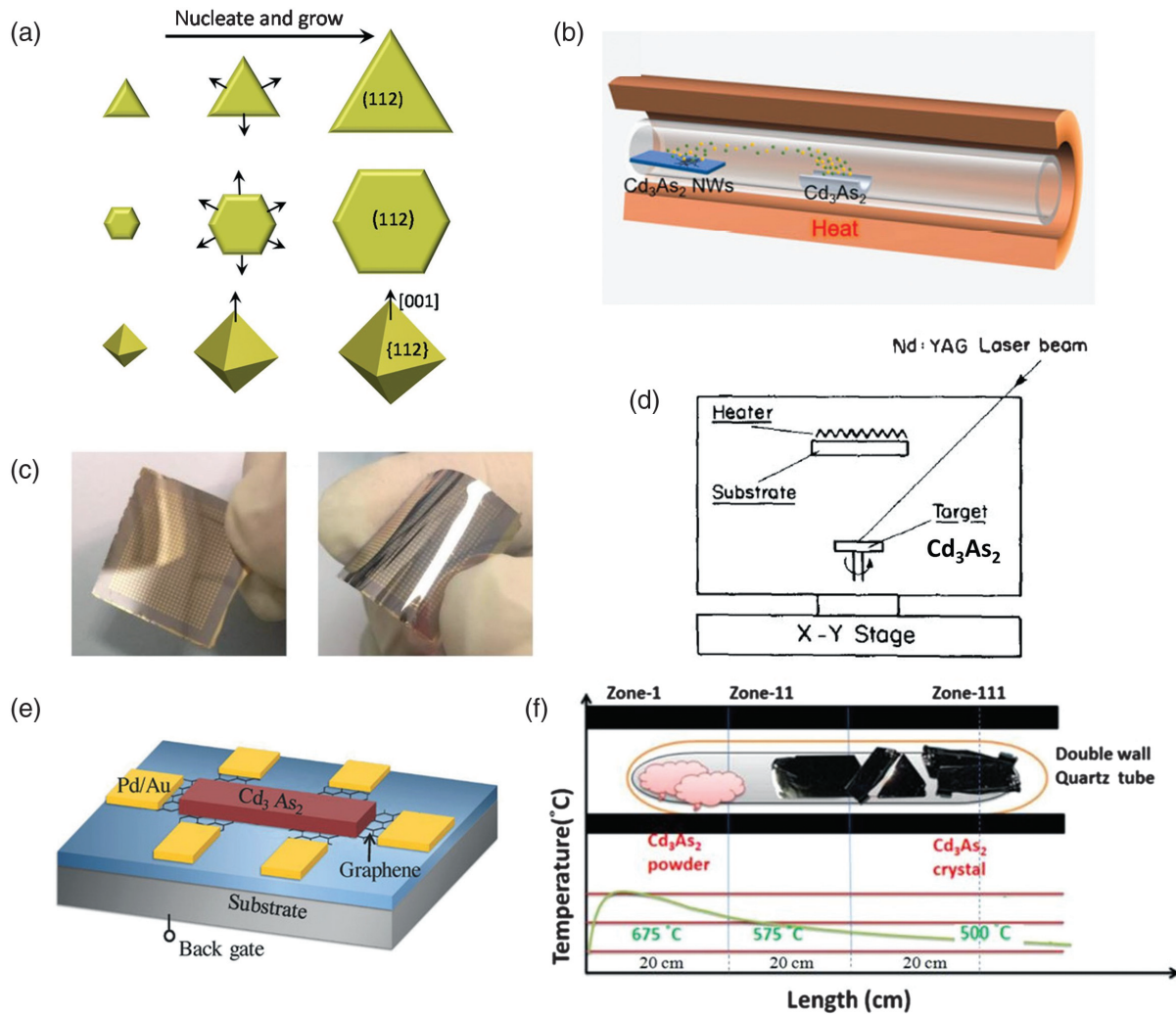
Fig. 2 Experimental methodologies to grow Cd_3As_2 nanostructures, thin films, single crystals, and fabrication of Cd_3As_2-based devices. (a) Schematic diagram of nucleation and growth process of Cd_3As_2 nanostructures by PVD. (b) Flow diagram of CVD growth of nano-wires. (c) Display of Cd_3As_2/organic thin films based device fabricated by MBE, showing excellent flexibility. (d) Schematic diagram of pulsed laser deposition technique to grow Cd_3As_2 thin films. (e) Graphene/Cd_3As_2 based heterostructure device fabricated by the CVD method. (f) SSVG system to grow single crystal Cd_3As_2. The figure is reproduced with the permission of (a) Ref. 44 © 2015 American Physical Society, (b) Ref. 50 © 2021 Springer Nature, (c) Ref. 46 © 2019 American Physical Society, (d) Ref. 51 © 1984 Elsevier, (e) Ref. 52 © 2021 Wiley-VCH GmbH, and (f) Ref. 53 © 2015 Nature Publishing Group.

characteristics make CVD the preferred method for synthesizing Cd_3As_2 nanostructures with diversely controlled morphologies. Zhang et al.[43] synthesized Cd_3As_2 nanostructures with various morphologies, including nanowires, nanoribbons, nanobelts, nanoplates, and nano-octahedrons, using a simple CVD process. The schematic of the CVD growth mechanism of Cd_3As_2 nanowires can be visualized by Fig. 2(b). All of these morphologies may be adjusted by altering the working chamber's pressure and argon gas flow rate. Magnetoresistance investigation showed that CVD-grown Cd_3As_2 nanostructures with diverse morphologies are advantageous for future nanoelectronic applications of DSM. Wu et al.[52] fabricated graphene/ Cd_3As_2 heterostructures [Fig. 2(e)] by CVD and observed a significant interlayer charge transfer that helped modify the Fermi level of graphene via

Cd_3As_2. These heterostructures have potential spintronics uses. The CVD fabricated Cd_3AS_2/WS₂ heterostructure-based photodetectors presented excellent performance with a high on–off ratio (5.3×10^4), responsivity (223.5 AW^{-1}) at 520 nm, and an outstanding detectivity (2.05×10^{14} Jones) at 808 nm in near infrared (IR) band.[57]

3.5 Self-Selecting Vapor Growth Technique

The self-selecting vapor growth (SSVG) method is a sealed tube method, suitable to grow single crystals of 3D DSM Cd_3As_2. The main distinctive advantage of this method is that the polycrystalline source material acts as a seed.[59] In this method, the growth capsule remains static and transportation of vapors is

Table 1 Growth conditions for Cd_3As_2 thin films, nanostructures, and single crystals for various growth techniques.

Material	Preparation method	Precursor/target	Growth temperature	Substrate	Reference
Cd_3As_2 thin film	PLD	Mixture of 6N5 Cd and 7N5 As shots target	Room temperature	$SrTiO_3$	Ref. 45
Cd_3As_2 thin film	PLD	Single crystal Cd_3As_2 target	Room temperature	Fused quartz plates	Ref. 51
Cd_3As_2 nanostructures	PVD	Cd_3As_2 powder	650°C	SiO_2/Si	Ref. 44
Cd_3As_2 thin film	MBE	Cd_3As_2 bulk	170°C	Mica	Ref. 21
Cd_3As_2 thin film	MBE	Cd_3As_2 target	140°C	CdTe	Ref. 60
Cd_3As_2 thin film	MBE	Cd_3As_2 target	150°C to 170°C	GaAs	Ref. 49
Cd_3As_2 thin film	MBE	Cd_3As_2 target	180°C	GaAs (111)B	Ref. 61
Cd_3As_2 nanostructures	CVD/ vapor solid mechanism	Cd_3As_2 powder	760°C	Si	Ref. 47
Cd_3As_2 nano-belts	CVD	Cd_3As_2 powder	760°C	Quartz	Ref. 52
Cd_3As_2 microbelts	CVD	Cd_3As_2 powder	760°C	Si	Ref. 58
Cd_3As_2 submicron wires	CVD	Cd_3As_2 powder (6N pure)	Upstream: 650°C Downstream: 350°C	SiO_2/Si coated with L BiI_3/ ethanol solution	Ref. 62
Cd_3As_2 single crystals	CVD	Cd and As powders	825°C	—	Ref. 63
Cd_3As_2 single crystals	SSVG	Stoichiometric mixture of Cd and As elements	850°C	—	Ref. 53

carried out by a small temperature gradient. The key feature of this deposition method is that material evaporates from the hotter part source material and recondensed on the cooler part by itself.[53] This process makes it possible to selectively generate crystal grains, resulting in the production of stress-free single crystals of increasing size and decreasing quantity.[53,59] The little variation in temperature between the evaporation and deposition portions of the source material is another essential aspect of this approach. Due to this small temperature difference, the driving force for distillation-like separation is low, and crystals produced under these conditions exhibit minimal compositional separation.[59] Sankar et al.[53] reported the formation of huge plate-shaped single crystals of Cd_3As_2 in an alumina furnace using the SSVG technique. Figure 2(f) is a cross-sectional view of the SSVG alumina furnace used for the creation of single crystal Cd_3As_2.

The experimental conditions including experimental methods, precursors/targets, substrates, and growth temperatures for the growth of Cd_3As_2 thin films, nanostructures, and single crystals are briefly summarized in Table 1. In addition, the comparison of the advantages and disadvantages of various fabrication techniques is tabulated in Table 2.

4 Photonics with 3D DSM Cd_3As_2

4.1 Optical Harmonic Generation in Cd_3As_2

Optical harmonic generation (OHG) is a nonlinear phenomenon that is utilized to investigate low-dimensional physics.[68] It is employed in the field of bioimaging, optical signal processing, and the development of innovative coherent light sources.[69] The study of these interactions is the heart of nonlinear optics, and a cornerstone of modern photonics. In particular, the extreme sensitivity of OHG to material characteristics, crystallinity, and defects, as well as its dependency on excitation parameters,

permits a diverse array of applications and nonlinear optical devices.[70–73] Conventional nonlinear devices are comprised of bulk materials such as beta barium borate (BBO), potassium titanyl phosphate (KTP), or lithium niobate ($LiNbO_3$).[70] On-chip integration and multifunctional or tunable devices are not feasible with these materials.[74,75] Plasmonic materials have been presented as nonlinear materials due to their ability to significantly increase nonlinear processes by restricting the field to a nanometric area.[76–79] Due to their significant dissipative losses, they are not suitable for nonlinear materials.[80] High-index dielectric nanomaterials have been introduced as a favorable alternative because of their strong magnetic response and low losses.[81,82] Despite these advancements, the effectiveness of nonlinear effects in these metasurfaces or nanostructures still falls short of the requirements of current nonlinear devices.[74] After discovering graphene in 2004,[83] much effort has been made to uncover the nonlinear physics in other 2D materials beyond graphene.[70,71,73,84] The enormous nonlinear coefficients of these atomically thin materials may allow them to replace conventional nonlinear media in photonic systems. A comparison of different materials in producing OHG is provided in Table 2. We are well aware that an exact comparison of $\chi^{(3)}$ requires consideration of a number of elements, including the working wavelength, manufacturing technique, substrate, and thickness. Each of these factors has a substantial influence on the $\chi^{(3)}$. We have used a typical value of $\chi^{(3)}$ to get an approximate estimate of $\chi^{(3)}$. Due to the fact that graphene and Cd_3As_2 (3D equivalent of graphene) are centrosymmetric, only $\chi^{(3)}$ values are considered in Table 3.

In 2020, terahertz-field-driven high-harmonic generation (HHG) in Cd_3As_2 was demonstrated experimentally at ambient temperature.[32] The third-, fifth-, and seventh-order harmonic generation were extremely efficient when excited by linearly polarized multicycle terahertz pulses and identified using time-resolved spectroscopic methods, as provided in Fig. 3(b).

**Table 2** The advantages and disadvantages of various fabrication techniques for the fabrication of Cd$_3$As$_2$.

Sr. No	Fabrication technique	Advantage	Disadvantage	Reference
1	Molecular beam epitaxy	1. Deposition is carried out in ultrahigh vacuum (up to 10^{-10} mbar). 2. High-quality large-area epitaxial Cd$_3$As$_2$ thin films can be grown with controlled thickness. 3. Good capacity to produce Cd$_3$As$_2$ heterostructures and superlattices with abrupt interfaces.	1. It causes poor crystallinity of material (Cd$_3$As$_2$) due to low growth temperature.	Refs. [45], [46], [64], [65]
2	Pulse laser deposition	1. Suitable for the growth of materials (Cd$_3$As$_2$) with high melting points, complicated stoichiometry, and sandwich architectures. 2. Can be operated in both inert and ultrahigh vacuum. High deposition rates and takes short time for deposition.	1. It causes nonuniformity of particulate size across the surface of Cd$_3$As$_2$ films due to the presence of molten material in the ablated material. 2. There is a possibility of splashing and formation of microsized island on the surface of deposited film.	Refs. [45], [55], [65]–[67]
3	Chemical vapor deposition	1. Feasible to synthesize both Cd$_3$As$_2$ thin films and nanostructures. 2. Versatile, adaptable, compatible, simplest, reproducible, productive, and cost effective technique.	1. Limited capacity to produce heterostructures and superlattices of Cd$_3$As$_2$ with abrupt interfaces. 2. Film thickness is not easy to control. 3. In CVD, deposition at high temperatures cause stresses in the Cd$_3$As$_2$ thin films and limits the choice of substrates.	Refs. [43], [52], [58]
4	Physical vapor deposition	1. It is suitable to synthesize both Cd$_3$As$_2$ thin films and nanostructures. 2. It involves both thermal heating and kinetic ejection of target material. 3. Film thickness control is easy and it is environment friendly and easy to use.	1. Low deposition rates. 2. Difficulty in evaporating and formation of alloys thin films. 3. It is extremely difficult to control stoichiometry of Cd$_3$As$_2$ thin films.	Refs. [44], [45], [56]
5	Self-selecting vapor growth	1. Suitable to grow Cd$_3$As$_2$ single crystals. 2. It involves little variation in temperature between the evaporation and deposition portions.	1. The growth process for Cd$_3$As$_2$ is very slow and deposition can take place a week to form. 2. The crystal shape of Cd$_3$As$_2$ is not controllable. 3. Scale-up beyond 8 cm^3 has not been demonstrated.	Refs. [53], [59]

Further investigation of the reported harmonic radiation is performed as a function of pump-pulse fluence. In the perturbative regime, their fluence dependency deviates significantly from the anticipated power-law dependence. Similarly, one more group observed a significant THz HHG in thin films of Cd$_3$As$_2$ at ambient temperature.[95] It was demonstrated that third harmonic generation (THG) can be detectable using a tabletop light source and can be as strong as 100 V cm^{-1} when a fundamental field of 6.5 kV cm^{-1} is applied within the film, exhibiting an exceptional efficiency for terahertz frequency conversion. In the same year, Ullah et al.[93] performed the THG investigation in Cd$_3$As$_2$ thin films. They measured THG in two types of fabricated devices at telecommunication wavelengths. In one device, Cd$_3$As$_2$ is fabricated on a mica substrate, while in the other, a micro planar cavity is embedded underneath the Cd$_3$As$_2$. They discovered a significant increase in the THG signal of up to 420 times in the device with a planar cavity compared with the device with bare Cd$_3$As$_2$ thin film on a mica substrate. On comparing the THG signal and $\chi^{(3)}$ of Cd$_3$As$_2$, glass, MoS$_2$, and graphene under the same measurement conditions [Fig. 3(d)], it was determined that the Cd$_3$As$_2$ has a $\chi^{(3)}$ value of 2.3×10^{-19} m^2 V^{-2}, which is 1000 times more than the $\chi^{(3)}$ value of glass and 1.3 and 1.5 times greater than the $\chi^{(3)}$ values of MoS$_2$ and graphene, respectively. Theoretically, the creation of HHG in 3D DSM via THz radiation has also been investigated recently.[33,94] It was demonstrated that 3D DSM is a promising solid-state platform for the highly efficient generation of extreme intraband-dominated THz harmonics up to the 31st order [Fig. 3(c)] and beyond using input field intensities of 10 MW/cm^2—a factor of $>10^5$ reduction in intensity over previous THz HHG demonstrations.[94] According to another study,[33] when a film thickness of 50 nm is increased to 1500 nm, the output intensities of the 3rd and 31st harmonics may be increased by factors of 144 and 28, respectively. More intriguingly, it was shown that highly nonlinear

Table 3 Comparison between Cd$_3$As$_2$ nonlinear efficiency with other materials including advantages and disadvantages.

Nonlinear material	Reference	$\chi^{(3)}$/m^2 V^{-2}	Phase control	Advantage	Disadvantage
Traditional bulk material (LiNbO$_3$)	Refs. 85, 86	$\sim10^{-21}$	No	Commercially available	Weak nonlinearity
Plasmonic nanostructures (gold)	Refs. 86–88	$\sim10^{-18} - 10^{-19}$	Yes	Strong field enhancement	High losses
Dielectric nanostructures	Refs. 89 and 90	$\sim10^{-20}$	Yes	Low losses	Moderate field enhancement
2D materials thin films	Refs. 69, 91, 92	$\sim10^{-18} - 10^{-19}$	Yes	1. Tunable 2. Easily integrated with other bulk structures	1. Due to atomic thickness the light–matter interaction is weak. 2. Making nanostructures is difficult
Cd$_3$As$_2$ thin film	Ref. 93	10^{-19}	Yes	1. Tunable 2. Extendable to other structures 3. Easy to make nanostructures	Need to be explored (Very few experimental findings and minimal understanding)
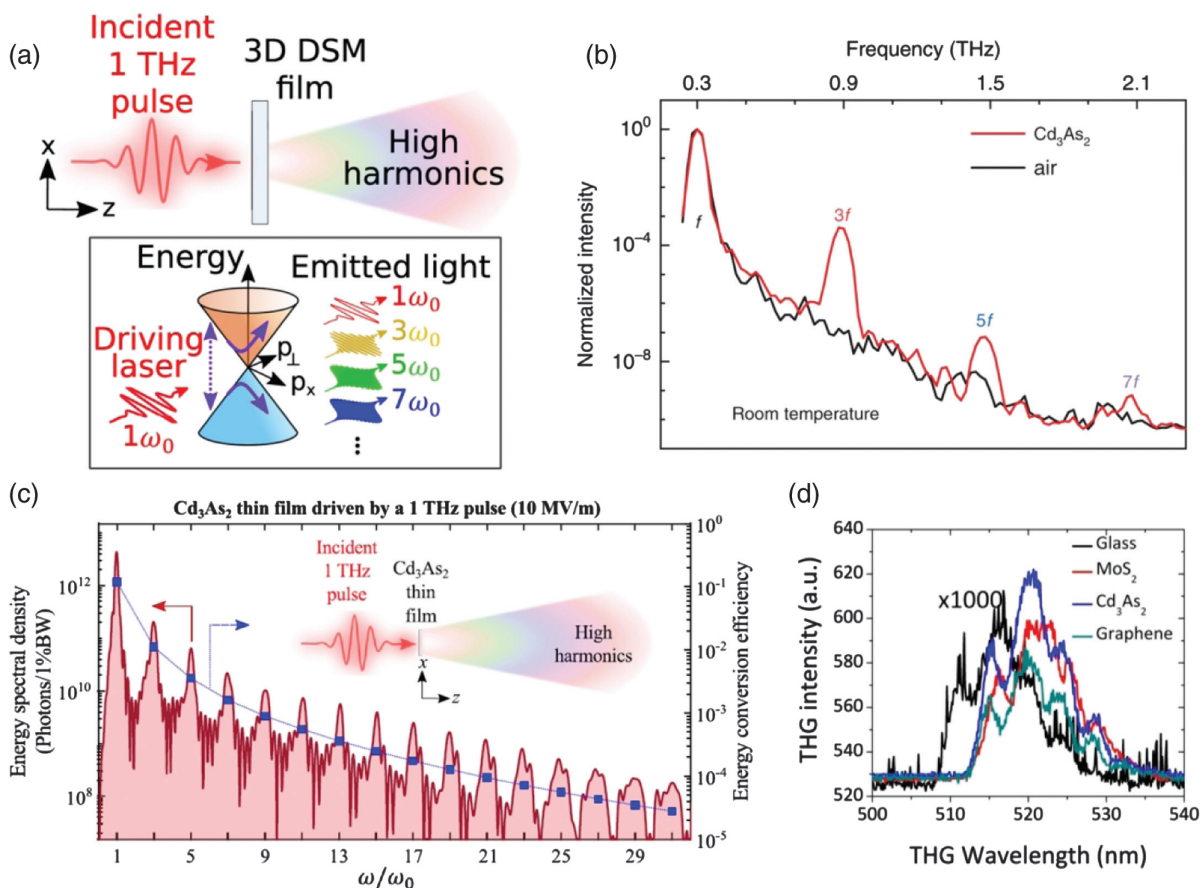
Fig. 3 OHG in 3D DSM Cd$_3$As$_2$. (a) Schematic demonstration of the generation of HHG from 3D DSM thin film. (b) Room temperature HHG in Cd$_3$As$_2$ film and air. (c) Theoretically estimated HHG in a 3D DSM thin film when a linearly polarized pulse with a central frequency of 1 THz and a peak field intensity of 10 MV/m generates harmonics up to the 31st order and beyond with energy conversion efficiency far over 10^{-5}. (d) A comparison of the THG signal among the Cd$_3$As$_2$, glass, MoS$_2$, and graphene. The figure is reproduced with the permission of (a) Ref. 33 © 2021 Nature Publishing Group, (b) Ref. 32 © 2020 Nature Publishing Group, (c) Ref. 94 © 2020 American Physical Society, and (d) Ref. 93 © 2020 AIP Publishing.

materials like 3D DSMs enable the appearance of a subwavelength phase-flip in the induced current density at nanoscale propagation lengths. This effect has not been seen in nonlinear materials that are typically used. There are a few additional theoretical publications[96,97] that explain the OHG in 3D DSM, including the second harmonic generation (SHG) in tilted DSMs with a broken tilt inversion symmetry when no external magnetic field is present.[97]
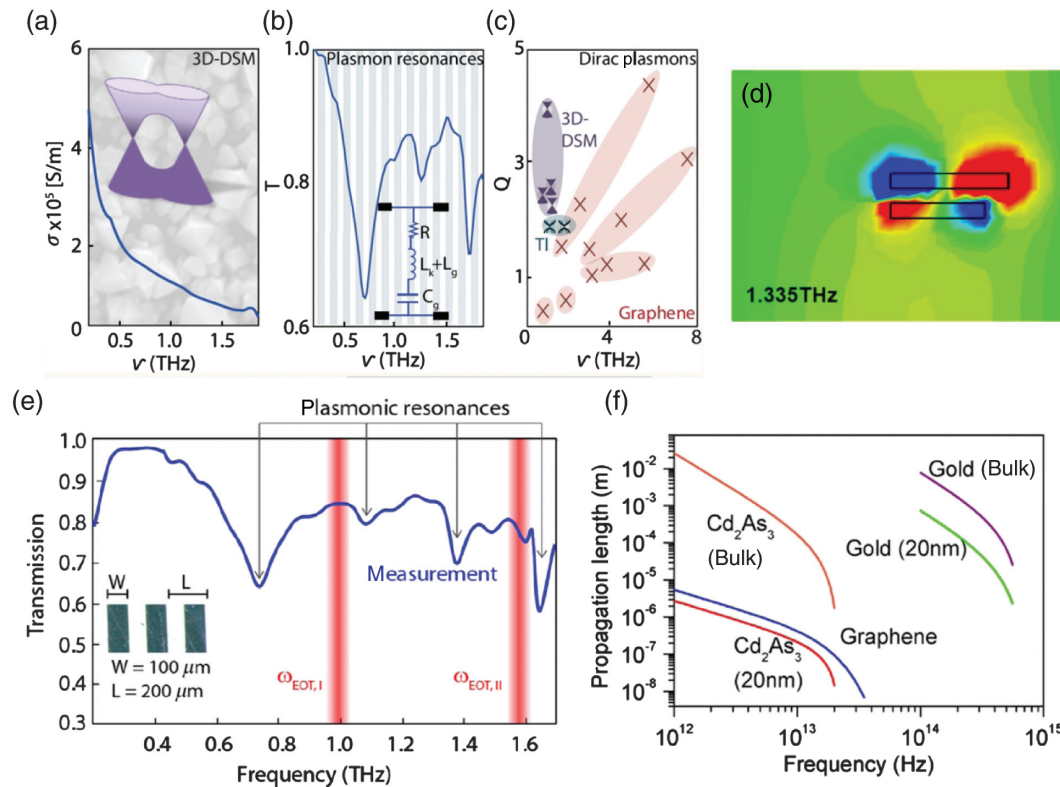
4.2 Plasmonics in Cd_3As_2

Recent advances in DSMs have focused attention on the strong coupling of electromagnetic radiation in these materials through plasmons. This enables subwavelength confinement and intense light–matter interaction, which is advantageous in a wide variety of nanophotonics applications.[98,99] There are two distinct characteristics of these plasmons. First, unlike parabolic band materials, these plasma oscillations are predominantly quantum mechanical in nature (since h is regarded as the leading term of the plasma dispersion relation). Additionally, these charge oscillations disappear when the Fermi level reaches the Dirac point ($E_F = 0$).[100] The second reason is that, in contrast to parabolic band materials, the linear energy dispersion in DSMs leads to a lower-order dependency of the plasmon resonance frequency (ω_p) on charge density (n), implying that plasmon resonances occur mostly at terahertz frequencies.[101] The existence of significant terahertz coupling in these materials, together with their ease of tuning and lengthy momentum scattering time (τ), has been envisioned to play a crucial role in the emerging area of terahertz electronics and optoelectronics. Up to the present, research efforts in this area have been primarily motivated by investigations of plasmons in 2D DSM graphene.[102] Interestingly, the recent experimental demonstration of long expected 3D counterparts of graphene[3,12–15] inspires additional research on electromagnetic phenomena and light–matter interaction, such as Dirac plasmons. In this aspect, the 3D character of 3D DSMs distinguishes them from their more often researched 2D counterparts.

Current theoretical research on plasmons in 3D DSMs reveals a fundamental difference in their dispersion relations when compared with 2D DSMs. The plasma frequency (ω_p) dependence in 3D DSM is $\omega_p \propto E_F \propto n^{1/3}$[103,104] whereas it results in $n^{1/4}$ in the case of 2D DSM.[101,102] The larger Fermi velocity in 3D DSM is very advantageous for creating plasmon resonances with a higher quality factor (Q).[101] This is comparable to the situation in parabolic band materials, where low effective masses and lengthy momentum scattering periods are linked with high quality factors in plasmonic resonances. The authors of a recent study[100] demonstrated that patterned Cd_3As_2 resonant plasmonic devices have spectrally narrow terahertz plasmon resonances [Fig. 4(a)]. This finding was ascribed to the extremely long momentum scattering time seen in Cd_3As_2 films, which is a direct result of the enormous v_F defining the Cd_3As_2 Dirac dispersion. Ooi et al.[19] reported that 3D DSM had the comparable nonlinear plasmonic performance to graphene while keeping the structural advantages of bulk metals, minimizing passive plasmonic losses, and being far simpler to handle in fabrication facilities. The surface plasmon propagation lengths of Cd_3As_2 were found to vary by up to three orders of magnitude between the bulk and thin film forms [Fig. 4(b)]. The same is true for bulk gold and thin gold films, whereas graphene, with a thickness of an atomic layer, has the same surface plasmon

propagation lengths as thin Cd_3As_2 films. Tunable propagation characteristics of 3D DSM-based hybrid plasmonic waveguides were explored.[106] The proposed hybrid waveguides exhibit strong (weak) confinement when the operating frequency is less (greater) than the transition frequency, due to the DSM layer's high plasmonic (dielectric low) loss feature. Similar plasmonic investigations in 3D DSM-based hybrid structures were investigated[107,108] in order to enhance the understanding of this topic.

Similarly, it was numerically demonstrated that 3D DSM is a flexible option for demonstrating the TE plasmonic mode.[109–113] The TE plasmon mode is often weakly limited and very difficult to see experimentally due to its sensitivity to the permittivity difference between adjacent materials.[114] The use of innovative low-dimensional materials, periodic multilayer structures, nonlinear materials, etc., helped to increase the TE plasmonic mode confinement and enable experimental observations.[115–118] For example, the spatial confinement of the TE plasmon was considerably increased by the 2D hexagonal boron nitrides layer, which was also very stable and existed even when the superstrate and substrate had a highly different permittivity.[116] With a graphene-metamaterials hybrid structure, the TE plasmon contributed significantly to the heat exchange and was effectively used to explore near-field radiative heat transfer.[117] The 3D DSM layer has a substantially greater thickness than graphene, making the TE plasmonic mode stronger and easier to create from an experimental standpoint. To investigate high-efficiency mid-IR spectral devices, a 3D DSM TE plasmonic structure has been investigated systemically, revealing that the obvious TE mode can be achieved when the Fermi level is not very large and the temperature is relatively high (about 100 K), in contrast to the graphene symmetric structure, which must operate at low liquid helium temperatures.[3,110,113,119–121] It was discovered that when the Fermi level rises, the transition frequency of TE modes increases and the peak location of the real and imaginary portions of effective indices exhibit evident blue shifts. At low temperatures, the interband transition contributes more, and the 3D DSM layer exhibits improved dielectric characteristics and enables a stronger TE mode.[122]

Plasmon-induced transparency (PIT) is a plasmon analogue of electromagnetically induced transparency. It is created by significant destructive interference between plasmon super-radiation and plasmon subradiation modes.[123,124] Its remarkable dispersion properties and wide range of uses have attracted researchers' curiosity. Recently, researchers presented a range of devices capable of producing the PIT effect. For instance, plasmonic waveguide coupled resonators, metamaterials, and metasurface structures have all been shown.[125–127] The majority of these devices are made of metallic materials, and it is almost hard to control the material's dielectric function and loss. Due to the metal's limited surface plasmons, modulation performance is exceedingly low. A dynamically tunable PIT effect is needed in real applications. Once constructed, the shape of the device is impossible to modify, and its singularity precludes practical usage. Additionally, few studies have been conducted on the tunable PIT effect. As previously mentioned, similar to graphene, the optical conductivity of 3D DSM may be tuned easily due to its structure. As a result, researchers produced a highly controllable PIT effect in metamaterials based on 3D DSM.[105,128] Chen et al.[129] also explored the multiband PIT effect. Additionally, a metamaterial based on 3D DSM was also reported that was very wide and tunable.[130] Certain researchers presented a waveguide

Fig. 4 Plasmonics in 3D DSM. (a) The variation of optical conductivity with a THz frequency in a Cd$_3$As$_2$ thin film. (b) Stripes of Cd$_3$As$_2$ thin film with a transmission spectrum demonstrating plasmonic resonances and an inset illustrating the transmission line model for transmission through a thin film ($t \ll \lambda$), where intraband conductivity can be modeled as series resistance, R, and kinetic inductance, L_k, which provides the Drude dispersion. (d) The distribution of the electric field at the z direction in a proposed PIT system at frequency of 1.335 THz. (e) Transmission spectra of a patterned stripe array showing plasmonic resonances for a Cd$_3$As$_2$ thin film whose dimensions are presented in the inset of this figure. (f) A comparison of surface plasmon propagation lengths between different plasmonic waveguides. The figure is reproduced with the permission of (a)–(c) and (e) Ref. 100 © 2019 American Chemical Society, (d) Ref. 105 © 2017 Optical Society of America, and (f) Ref. 19 © 2019 AIP Publishing.

structure device for implementing the PIT effect that is simpler to incorporate into an optical circuit than the metamaterials-based 3D DSM.[131]

4.3 Ultrafast Photocarrier Dynamics in Cd$_3$As$_2$

Generally, the ultrafast dynamics of a material referred to its response to the excitation of an optical pulse (either pump or probe) with a timescale of sub- and pico-seconds (ps). Both pulse types have a typical duration of 20 to 100 femtoseconds (fs).[132] When the sample comes into contact with the pump, its characteristics are momentarily altered, mostly via the excitation of electrons and phonons and the changing of the electronic band structure. It is possible to monitor the changes with a probe pulse that is delivered at a variable time after the pump: for example, by measuring the reflectivity, transmissivity, or photo-electron spectrum. Ultrafast experiments are set to play a critical role in the research and use of topological materials, most notably the 3D DSM.[133] The majority of the features of 3D DSM, including their linear band dispersion, Berry curvature, the near-vanishing density of states at Fermi energy, and sensitivity to crystalline and time-reversal symmetry, are intimately tied to

their sub- and few-picosecond reaction to light.[132] The ultrafast responses of numerous DSMs have been measured and are now in practical use. These materials were utilized to create a passive optical switch for picosecond mode-locking of a midinfrared laser[134] and broadband infrared photodetectors[46,135] with response times of a few picoseconds.

Weber et al.[136] determined the ultrafast transient grating properties of Cd$_3$As$_2$ at both room temperature and 80 K in 2015. Following photoexcitation with 1.5-eV photons, charge carriers undergo two relaxation processes, one lasting 500 fs and the other lasting 3.1 ps. The authors determined that by measuring the complex phase of the change in reflectance, the faster signal corresponds to a reduction in absorption and the slower signal to a drop in the phase velocity of light at the probe energy. The hot-carrier relaxation dynamics in Cd$_3$As$_2$ thin films was investigated by Zhu et al.[137] The combination of degenerate and nondegenerate pump-probe spectroscopy revealed that the hot carrier distribution in Cd$_3$As$_2$ is formed on a period of about 400 fs. Numerous studies on the dynamics of photocarriers in Cd$_3$As$_2$ were conducted utilizing ultrafast optical pump and optical probe spectroscopy in the visible and near-to-midinfrared regions.[17,134,137,138] Zhang et al.[113] used terahertz spectroscopy to
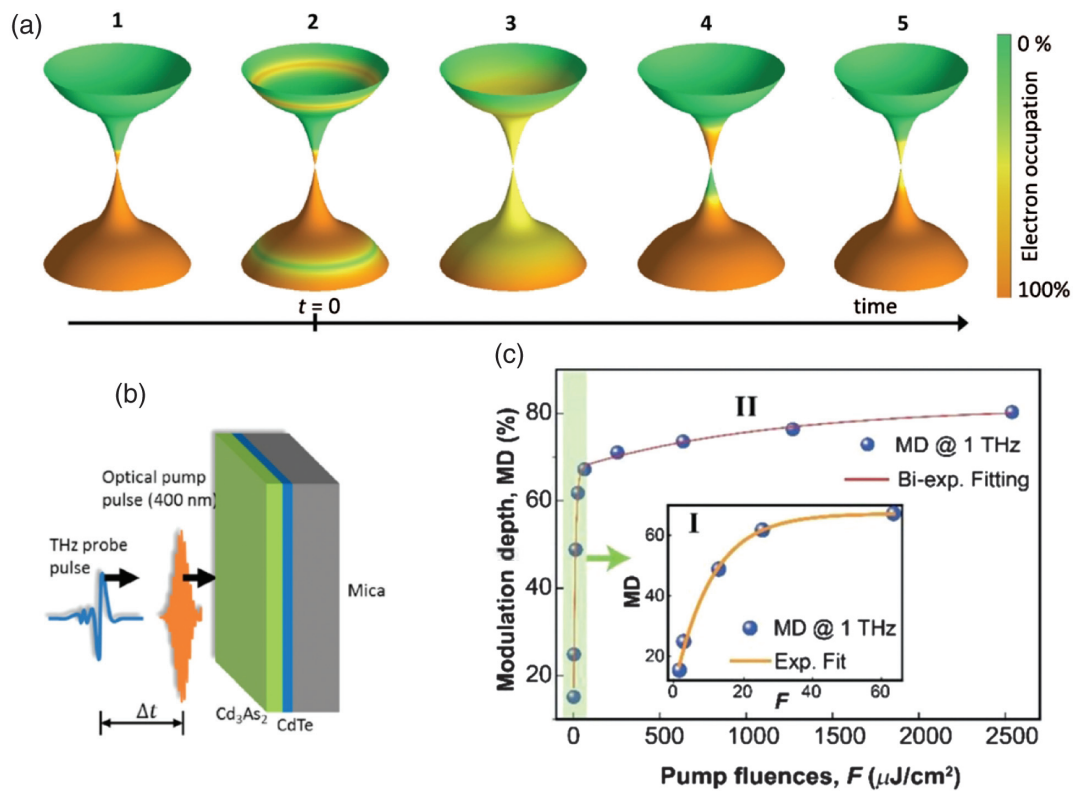
Fig. 5 Ultrafast photocarrier dynamics in 3D DSM: Cd$_3$As$_2$. (a) Schematic representation of the excitation and relaxation of electrons and holes from process 1 to 5 (1. before excitation, 2. immediately after excitation, 3. high-temperature thermal distribution, 4. partially cooled distribution with inverted populations, 5. a partially cooled, noninverted distribution). (b) The Cd$_3$As$_2$ sample structure is shown schematically with the illustration of optical pump THz probe spectroscopy. (c) The modulation depth (MD) at 1.0 THz versus pump fluences of Cd$_3$As$_2$ thin film at room temperature. The figure is reproduced with the permission of (a) Ref. 133 © 2017 AIP Publishing, (b) Ref. 113 © 2019 AIP Publishing, and (c) Ref. 23 © 2021 Wiley-VCH GmbH.

study the ultrafast photocarrier dynamics in a Cd$_3$As$_2$ thin film as can be visualized in Fig. 5(b). THz radiations have a very low photon energy, and optical pump and THz probe (OPTP) spectroscopy can be utilized to study photocarrier dynamics at the Fermi surface.[139] Time-resolved THz spectroscopy is a noncontact and noninvasive spectroscopy technique that enables the analysis of material's high-frequency photoconductive response on subpicosecond time scales. By evaluating the real and imaginary components of the complex conductivity spectrum, it is feasible to derive the development of both the concentration and mobility of charge carriers with ultrafast temporal precision. It was discovered[113] that using an optical pump may result in significant absorption in the Cd$_3$As$_2$ thin film at THz frequencies. Following photoexcitation, the maximal THz photoconductivity is obtained with a time constant of 1.0 ps that rises slightly with pump fluence, and the following decay proceeds by a single exponential relaxation with a typical lifespan of 6.0 ps, regardless of pump fluence. Another time-resolved terahertz spectroscopic study[23] in a Cd$_3$As$_2$ thin film at room temperature revealed a modulation depth of 63% at a record low optical fluence of 63.5 μJ cm^{-2} with an ultrafast switching time of 15.5 ps [Fig. 5(c)]. Several other studies[132,138,139] on photoexcitation dynamics in Cd$_3$As$_2$ were carried out by different researchers in order to enhance the understanding of this topic. Additional knowledge of the 3D DSM photoexcitation response

will be crucial for basic research, including establishing a predicted exciton condensate, linking photocurrents to electronic topology, closing or opening gaps at Dirac points, and converting nodal lines to point nodes.

4.4 Optical Absorption in Cd$_3$As$_2$

Absorption enhancement is a critical component of optical devices and has garnered much attention in recent years. Theoretically, a perfect absorber is created by limiting reflection and eliminating transmission. Since Landy et al.[140] first reported a flawless metamaterial-based absorber in 2008, metamaterial-based absorbers have been intensively explored and proven across a wide variety of spectral ranges, including microwave,[141] terahertz,[142] and infrared.[143] Their popularity stems from their versatility in a variety of applications, including thermo-photovoltaics,[76] sensors,[144–146] and filters,[147,148] as well as thermal radiation tailoring.[149,150] For the most part, an absorber is made up of a metal-dielectric-metal (MDM) structure, with the metal layer on top serving as an impedance matcher and the metal layer below serving as a transmission-blocking "salisbury screen," however, if the metal layer below is too thin, the MDM arrangement may be utilized as an optical device to boost transmission.[151] Due to radiative damping and nonradiative losses, these absorbers have very large absorption bandwidths,

which is advantageous for a broadband absorber. Fortunately, nonradiative losses may be decreased by replacing the upper metal layer with a low-loss material, such as a dielectric.[152,153] Unfortunately, ideal absorbers based on conventional noble metals such as gold, silver, or copper are constructed with fixed absorption peaks and must have their geometric parameters meticulously reoptimized if the absorption peaks have to be tuned to different frequency regions.[154]

2D materials have been employed to improve the absorber's stability and absorption. Graphene is one of the most widely used 2D materials and has shown great promise in metasurface applications.[155] Graphene's optical response is defined by its surface conductivity, which is related to its Fermi energy and may be modified dynamically using a bias voltage.[69] Various researchers have successfully achieved dynamically tunable perfect absorption using 3D DSM. For example, Liu et al.[156] suggested a narrowband absorber in 2018 that made use of the metallic feature of 3D DSM at THz frequencies and achieved a total quality factor Q of 94.6.[36] Similarly, when the Fermi level is between 65 and 85 meV and the resonance frequency is between 2.46 and 3.16 THz, tunable narrow band absorbers with >95% absorption have been obtained. Dai et al.[157] developed a broadband terahertz cross-polarization conversion based on 3D DSMs that can be controlled by adjusting the Fermi level of the 3D DSMs, with the polarization conversion rate typically exceeding 80%. Several other proposed designs of 3D DSM absorbers have been proposed including the ultrahigh Q tunable 3D DSM absorber[158] and triple band absorber[159] based on 3D DSM. These proposed designs for a 3D DSM absorber open new avenues for the construction of tunable absorbers and may have applications in photovoltaic technology.

4.5 Some Other Photonics of Cd₃As₂

Enhancing our knowledge of photonic modes in nanomaterials enables us to better understand the underlying processes involved in optoelectronic devices and optimize their performance. Surface waves have drawn considerable attention as types of photonic modes, including surface plasmon polaritons (SPPs) and quasicylindrical waves (QCWs).[160–163] The QCW is an optical field scattered by subwavelength indentations, distributed along a surface over several wavelengths, containing both radiative and evanescent components. The optical QCW on Cd₃As₂ nanoplates has recently been studied[164] by a team of researchers across a wide range of wavelengths from ultraviolet (UV) to visible. It was found that QCW is of the same wavelength as the input light and decays at a rate of $r^{1/2}$ from the scattering source. Transverse magnetic modes were found to dominate the QCW pattern, depending on the excitation polarization relative to the Cd₃As₂ nanoplate edges.[164] Additionally, numerical simulations indicated that the Cd₃As₂ metasurface may improve absorption when compared with naked nanoplates. This is advantageous with the aid of QCW, since the interference between the incoming light and QCW modes results in a stronger local field, which increases absorption.

In a recent paper,[16] the authors investigated the thermo-optic characteristics of epitaxially grown Cd₃As₂ using infrared spectroscopy and demonstrated significant optical tunability in the mid- and far-infrared regions [Fig. 6(d)]. The finding is significant since many of Cd₃As₂'s tunable optical and thermal characteristics remain unknown. Furthermore, understanding the dynamics of charge carriers perturbed by electromagnetic fields

is critical for understanding the underlying physics of optical excitations. It was proved that tuning the Fermi distributions results in a substantial infrared thermo-optic shift. The results described in this article may stimulate more studies into the tunable optical and electrical properties of Dirac and Weyl semimetals and may pave the way for novel applications in reconfigurable optoelectronic and nanoscale thermal devices.[16]

The coding metasurface idea entails the creation of arrays of coding unit cells having a phase response from 0 to 2π.[166] Then, by optimizing the coding sequence of the microstructures, the suggested metasurfaces may be utilized to flexibly alter electromagnetic waves.[167] For instance, two adjacent units with a phase difference of 180 deg correspond to two elements ('0' and '1' elements) of a one-bit coding hypersurface.[168] Recently, graphene was introduced for the purpose of fabricating tunable coding metasurfaces.[169,170] However, graphene's structure is very thin and is quickly altered by its dielectric surroundings. Additionally, fabricating graphene-based metasurfaces is challenging. In order to solve these issues, a switchable coding metasurface was developed to enable dynamic beam steering based on a 3D DSM in the THz frequency range.[165] It was shown that the suggested metamaterials unit cell's relative phase delay may be actively controlled by altering the Fermi level (E_F) of the 3D DSM. By varying the E_F value of the 3D DSM for the 1-bit coding metasurface, the coding units with "0" and "1" states may be turned on/off in the frequency range from 1.46 to 2 THz. In such 1-bit coding metasurfaces, the beam numbers and propagation direction of the reflected waves may be programmed arbitrarily. Additionally, a dynamically controlled two-bit coding metasurface based on 3D DSM microstructures was built into the work to enable more advanced beam modulation.

In response to the question of whether 3D DSMs have an intrinsic topological signature that can be seen in the optical spectrum, the answer may be connected to chiral anomalies, which is one of the distinguishing properties of these systems.[171] Optically, minimal experimental data, such as a significant Kerr rotation in Cd₃As₂,[172] has been demonstrated, although several theoretical approaches have been proposed about this feature. For observable experimental characteristics, however, low temperature and good quality samples are recommended, since high temperature and scattering processes induced by contaminants may smooth out these features.

5 Applications of Photonics of 3D DSM Cd₃As₂

Since the beginning of the 1990s, semiconductor saturable absorber mirrors (SESAMs) in the early 1990s have been a crucial technique in the near-infrared sector.[20] SESAM is one of the most essential saturable absorber technologies because of its adaptability and precision. It can be included in numerous laser formats, such as fiber, solid-state, and semiconductor chip lasers.[173–175] By monitoring the midinfrared optical response of the bulk Dirac fermions, it has been shown that MBE-grown Cd₃As₂ thin films may function as an efficient ultrafast (<10 ps) optical switch in the midinfrared, with a working range spanning at least from 3 to 6 μm.[20]

Ultrafast response time, broad wavelength range, and great sensitivity make photodetection ideal for optical communications, optical interconnects, imaging, and remote sensing, among other optoelectronic and photonic applications.[17] An outstanding photodetector based on graphene has demonstrated
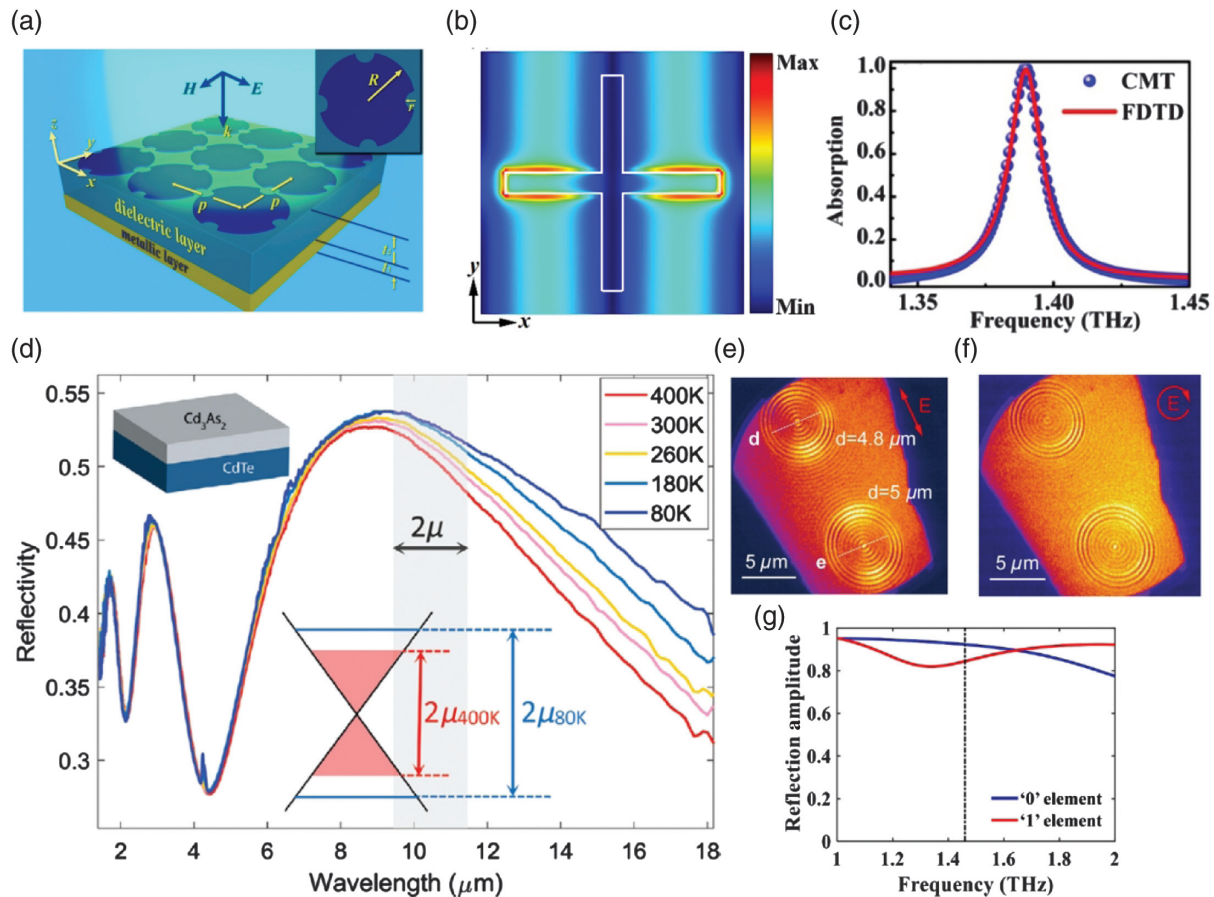
Fig. 6 Perfect absorption using 3D DSM and some other photonic properties. (a) A schematic of the perfect absorber composed of a patterned 3D DSM film, the dielectric layer, and a metal reflector. (b) Calculated electric field distribution of a crossed shape absorber composed of 3D DSM. (c) Simulated absorption of a metamaterial absorber based on 3D DSM. (d) Measured reflectivity of Cd$_3$As$_2$ at various temperatures. The reflectance of gold was used to normalize all measurements. (e) and (f) Static photoemission electron microscopic (PEEM) image of fabricated Cd$_3$As$_2$ nanostructures excited by a linear-polarized 410 nm laser pulse (e) and circularly polarized light (f). The polarization is manifested by the red arrow. (g) Reflection amplitude of a coding unit cell of 0 and 1 of metasurface made with 3D DSM. The figure is reproduced with the permission of (a) Ref. 154 © 2019 Optical Society of America (OSA), (b) Ref. 158 © 2021 MDPI, (c) Ref. 156 © 2018 Optical Society of America (OSA), (d) Ref. 16 © 2020 Wiley-VCH GmbH, (e) and (f) Ref. 164 © 2022 Wiley-VCH GmbH, and (g) Ref. 165 © 2022 Elsevier.

tremendous promise for fast operating speeds, broadband responsiveness, and efficient carrier multiplications, all of which benefit from its linear dispersion band structure with high carrier mobility and zero bandgap. As the 3D equivalent of graphene, DSM Cd$_3$As$_2$ has all of graphene's benefits as a photosensitive material but can interact with light more strongly as a bulk material, resulting in increased reactivity. Various 2D materials-based photodetectors can significantly suppress dark current and the efficient photon absorption from the visible to near-IR region, resulting in an enormously enhanced photoresponse. Due to their nearly gapless band structure, topological materials are able to achieve low-energy photon absorption; as a result, photodetectors based on these materials have an enormous advantage in terms of detection range, up to the far-infrared and terahertz range.[20] Among all other topological semimetals, Cd$_3$As$_2$ is easy to synthesize and is highly stable in air atmosphere.[93] The simple development of Cd$_3$As$_2$ thin film

and its compatibility with other semiconducting materials make it suitable for use in infrared cameras and wide-band photodetection.[176] On the other hand, its nearly zero bandgap gives rise to a larger dark current and adversely affects the responsivity of the device. To suppress the dark current and improve the responsivity, the heterostructure of Cd$_3$As$_2$ with other materials can be formed. The rectification effect of the heterostructure and the effective charge carrier separation lead to suppress the dark current and hence improved responsivity of photodetector.[176] In this work,[17] the development of a Cd$_3$As$_2$-based ultrafast broadband photodetector was discussed. Without any device optimization, the prototype metal-Cd$_3$As$_2$-metal photodetector exhibited a responsivity of 5.9 mA/W and a response time of around 6.8 ps. It was possible to generate broadband responses from 532 nm to 10.6 m, with a potential detection range extending to far infrared and terahertz. However, the high conductivity of prototype metal-Cd$_3$As$_2$-metal photoelectric devices
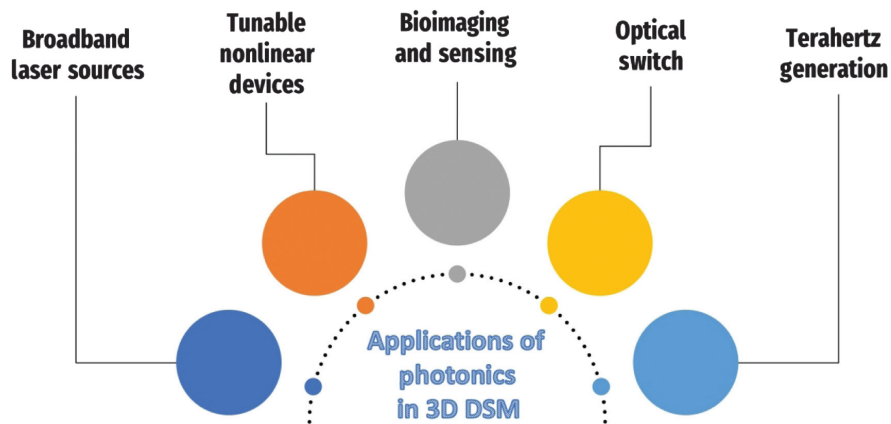
Fig. 7 Schematic shows the potential applications that can generate with the photonics of 3D DSM Cd_3As_2.

generates a substantial dark current, which significantly limits the enhancement of performance characteristics such as responsivity and detectivity. To overcome this limitation and enhancing the parameters of photoelectric devices, Cd_3As_2/semiconductor heterostructure-based fast photodetection devices have emerging applications in modern optoelectronic industry.[176] In comparison to the metal-Cd_3As_2-metal device, the Cd_3As_2/CuPc (copper-phthalocyanine) heterostructure based photodetector recently shown superior figure of merit.[177] Under irradiation of 808 nm, the Cd_3As_2/CuPc heterostructure-based device showed optimal values of performance parameters including detectivity (7.83×10^{10} jones) and responsivity (142.5 AW^{-1}) that are much enhanced as compared with the detectivity (7.79×10^9 jones) and responsivity (4.65 AW^{-1}) of pure metal-Cd_3As_2-metal device.[177]

Due to its high carrier mobility and variable carrier concentration, Cd_3As_2 provides an attractive possibility for high performance applications, such as plasmonics and optoelectronic devices based on 3D DSM plasmons.[19] In contrast to noble metal plasmons, 3D DSM Cd_3As_2 plasmons[19,178] are broadband and display exceptionally strong confinement, enabling light-matter interaction for quantum optics, chemical identification, and biosensors.[20] Importantly, the tune-able surface conductivity expands the application potential of Cd_3As_2. There are various photonic uses of Cd_3As_2 such as tunable absorber[157,158] and polarizer,[157] that make it a perfect choice in tunable photonic systems. Figure 7 depicts a schematic illustration of the use of the photonics of 3D DSM Cd_3As_2.

6 Conclusions and Future Perspectives

We have discussed most recent developments in numerous photonic aspects related to 3D DSM Cd_3As_2, and in particular, cutting-edge photonic technologies based on 3D DSM Cd_3As_2 such as linear and nonlinear plasmonics, optical absorption, optical harmonic generation, ultrafast dynamics, and several others. In addition, we have included a short review of current developments in Cd_3As_2 synthesis methodologies. Reviewing its optical characteristics revealed that Cd_3As_2 is a notable member of the topological materials class, which has been extensively investigated using both theory and experiment. There is no question that Cd_3As_2 contains well-defined 3D massless charge carriers.

Without a doubt, 3D DSM will continue to draw the interest and effort of researchers. However, the synthesis of large-area, high-quality materials is always necessary not just for the demonstration of intriguing topological physics, but also for mass-scale device applications. In order to go ahead, methods of measuring and controlling must be devised. In reality, the creation of probes is necessary to fully understand many unusual quantum states. It may be necessary to use a variety of strategies under extreme conditions to make the most of these tools. Quantum control of the physics is another route that may be attainable via the integration of electrical and optical methods, resulting in practical applications. In particular, it is necessary to create approaches at various frequencies, particularly in the GHz and THz ranges, that are tuned to the fascinating topological quantum physics. Since the Cd_3As_2/pentacene heterojunction[179] device may increase the responsivity and external quantum efficiency in a wide range from visible light to far-infrared light, it is viable to employ heterostructures of Cd_3As_2 and organic molecules to create photodetectors. Along this path, we anticipate achieving devices with greater responsiveness and external quantum efficiency using various organic compounds, as well as significantly expanding the responsive range (toward THz). In addition, it seems that the effort to use Cd_3As_2 as a saturable absorber in the area of pulsed lasers is effective. Cd_3As_2 is a highly adaptable near-infrared SESAM as a result of its primary properties, which include wide scalability, broadband functioning, and variable parameter control. We foresee the development of the suggested electrically contacted saturable absorber device. It may be extended further to active photonic devices working in the near-to-far-infrared spectrum, such as optical modulators and tunable light-emitting devices. In contrast to 2D semiconductors, which have been widely investigated, large-area 3D DSM Cd_3As_2 fabrication experience is currently scarce. A general way to generate high-quality, wafer-scale films at a cheap cost and with a high yield has not yet been established, even though numerous fabrication processes have been reported.[48]

Cd_3As_2 heterostructure-based photodetectors exhibit stronger and broadband photo-responsivity from the UV to far-IR regions. The IR imaging of Cd_3As_2 is an extremely important step to raise the research level of 3D DSM for practical applications. In the future, more Cd_3As_2 heterostructures can be designed to improve the responsivity and provide more solid foundations for its applications. Reduction in the carrier concentration of electrons in Cd_3As_2 can enhance the lifetime of photo-generated

carriers and allows more to reach the interface. To identify the ways to reduce electron concentration in as-grown highly n-type Cd_3As_2 will be an important step. Utilization of transparent electrodes can improve the collection of photogenerated carriers, enhancing the number of photons reaching the junction.[176] Progress in the growth of large area Cd_3As_2 with high quality and integrability will improve over the coming years and will significantly improve the key device characteristics such as responsivity and detectivity.[48] This will provide a pathway for Cd_3As_2 to become an essential part of viable optoelectronic devices. Clearly, the investigation of the optical properties possessed by 3D DSM Cd_3As_2 is still in its infancy, and we may be on the verge of discovering something a great deal stranger than what we had envisioned.

Acknowledgments

References

1. N. P. Armitage, E. J. Mele, and A. Vishwanath, "Weyl and Dirac semimetals in three-dimensional solids," *Rev. Mod. Phys.* **90**(1), 15001 (2018).
2. X. L. Qi and S. C. Zhang, "Topological insulators and superconductors," *Rev. Mod. Phys.* **83**(4), 1057–1110 (2011).
3. Z. K. Liu et al., "A stable three-dimensional topological Dirac semimetal Cd_3As_2," *Nat. Mater.* **13**(7), 677–681 (2014).
4. F. Ceballos and H. Zhao, "Ultrafast laser spectroscopy of two-dimensional materials beyond graphene," *Adv. Funct. Mater.* **27**(19), 1604509 (2017)
5. T. Jiang et al., "Gate-tunable third-order nonlinear optical response of massless Dirac fermions in graphene," *Nat. Photonics* **12**(7), 430–436 (2018).
6. K. F. Mak et al., "Optical spectroscopy of graphene: from the far infrared to the ultraviolet," *Solid State Commun.* **152**(15), 1341–1349 (2012).
7. H. A. Hafez et al., "Extremely efficient terahertz high-harmonic generation in graphene by hot Dirac fermions," *Nature* **561**(7724), 507–511 (2018).
8. H. A. Hafez et al., "Terahertz nonlinear optics of graphene: from saturable absorption to high-harmonics generation," *Adv. Opt. Mater.* **8**(3), 1900771 2020.
9. F. Bonaccorso et al., "Graphene photonics and optoelectronics," *Nat. Photonics* **4**(9), 611–622 (2010).
10. C. N. R. Rao et al., "Graphene: the new two-dimensional nanomaterial," *Angew. Chemie Int. Ed.* **48**(42), 7752–7777 (2009).
11. M. Liu et al., "A graphene-based broadband optical modulator," *Nature* **474** (7349), 64–67 (2011).
12. S. Borisenko et al., "Experimental realization of a three-dimensional Dirac semimetal," *Phys. Rev. Lett.* **113**(2), 027603 (2014).
13. M. Neupane et al., "Observation of a three-dimensional topological Dirac semimetal phase in high-mobility Cd_3As_2," *Nat. Commun.* **5**, 3786 (2014).
14. Q. Li et al., "Chiral magnetic effect in $ZrTe_5$," *Nat. Phys.* **12**(6), 550–554 (2016).
15. Z. K. Liu et al., "Discovery of a three-dimensional topological Dirac semimetal, Na_3Bi," *Science* **343**(6173), 864–867 (2014).
16. H. T. Chorsi et al., "Widely tunable optical and thermal properties of Dirac semimetal Cd_3As_2," *Adv. Opt. Mater.* **8**(8), 1901192 (2020).
17. Q. Wang et al., "Ultrafast broadband photodetectors based on three-dimensional Dirac semimetal Cd_3As_2," *Nano Lett.* **17**(2), 834–841 (2017).
18. Y. Meng et al., "Three-dimensional Dirac semimetal thin-film absorber for broadband pulse generation in the near-infrared," *Opt. Lett.* **43**(7), 1503 (2018).
19. K. J. A. Ooi et al., "Nonlinear plasmonics of three-dimensional Dirac semimetals," *APL Photonics* **4**(3), 034402 (2019).
20. Y. K. Yang et al., "Electrical transport and optical properties of Cd_3As_2 thin films," *Chin. Phys. B* **28**(10), 107502 (2019).
21. Y. Liu et al., "Gate-tunable quantum oscillations in ambipolar Cd_3As_2 thin films," *NPG Asia Mater.* **7**(10), e221 (2015).
22. C. Shekhar et al., "Extremely large magnetoresistance and ultra-high mobility in the topological Weyl semimetal candidate NbP," *Nat. Phys.* **11**(8), 645–649 (2015).
23. Z. Dai et al., "High mobility 3D Dirac semimetal (Cd_3As_2) for ultrafast photoactive terahertz photonics," *Adv. Funct. Mater.* **31**(17), 2011011 (2021).
24. W. Zhang et al., "Topological aspect and quantum magnetoresistance of β-Ag_2Te," *Phys. Rev. Lett.* **106**(15), 156808 (2011).
25. H. Li et al., "Negative magnetoresistance in Dirac semimetal Cd_3As_2," *Nat. Commun.* **7**, 10301 (2016).
26. C. Liu et al., "Oscillatory crossover from two-dimensional to three-dimensional topological insulators," *Phys. Rev. B - Condens. Matter Mater. Phys.* **81**(4), 041307 (2010).
27. S. Suetsugu et al., "Giant orbital diamagnetism of three-dimensional Dirac electrons in Sr_3PbO antiperovskite," *Phys. Rev. B* **103**(11), 115117 (2021).
28. Z. Wang et al., "Three-dimensional Dirac semimetal and quantum transport in Cd_3As_2," *Phys. Rev. B - Condens. Matter Mater. Phys.* **88**(12), 125427 (2013).
29. X. Wan et al., "Topological semimetal and Fermi-arc surface states in the electronic structure of pyrochlore iridates," *Phys. Rev. B - Condens. Matter Mater. Phys.* **83**(20), 205101 (2011).
30. Z. Wang et al., "Dirac semimetal and topological phase transitions in A 3Bi (A=Na, K, Rb)," *Phys. Rev. B - Condens. Matter Mater. Phys.* **85**(19), 195320 (2012).
31. L. Fu and C. L. Kane, "Superconducting proximity effect and Majorana fermions at the surface of a topological insulator," *Phys. Rev. Lett.* **100**(9), 096407 (2008).
32. S. Kovalev et al., "Non-perturbative terahertz high-harmonic generation in the three-dimensional Dirac semimetal Cd_3As_2," *Nat. Commun.* **11**, 2451 (2020).
33. J. Lim et al., "Maximal terahertz emission in high harmonic generation from 3D Dirac semimetals," *Commun. Phys.* **4**(1), 4–10 (2021).
34. I. Crassee et al., "3D Dirac semimetal Cd_3As_2: a review of material properties," *Phys. Rev. Mater.* **2**(12), 120302 (2018).
35. O. V. Kotov and Y. E. Lozovik, "Dielectric response and novel electromagnetic modes in three-dimensional Dirac semimetal films," *Phys. Rev. B* **93**(23), 235417 (2016).
36. M. Ali et al., "The crystal and electronic structures of Cd_3As_2, the three-dimensional electronic analogue of graphene," *Inorg. Chem.* **53**(8), 4062–4067 (2014).
37. A. Pietraszko and K. Łukaszewicz, "Thermal expansion and phase transitions of Cd_3As_2 and Zn_3As_2," *Phys. Status Solidi* **18**(2), 723–730 (1973).
38. G. A. Steigmann and J. Goodyear, "The crystal structure of Cd_3As_2," *Acta Crystallogr. Sect. B Struct. Crystallogr. Cryst. Chem.* **24**(8), 1062–1067 (1968).
39. B. Xu et al., "Optical spectroscopy of the Weyl semimetal TaAs," *Phys. Rev. B* **93**(12), 121110 (2016).
40. A. B. Sushkov et al., "Optical evidence for a Weyl semimetal state in pyrochlore $Eu_2Ir_2O_7$," *Phys. Rev. B - Condens. Matter Mater. Phys.* **92**(24), 241108 (2015).
41. D. Neubauer et al., "Interband optical conductivity of the [001]-oriented Dirac semimetal Cd_3As_2," *Phys. Rev. B* **93**(12), 121202 (2016).

42. T. Liang et al., "Ultrahigh mobility and giant magnetoresistance in the Dirac semimetal Cd₃As₂," *Nat. Mater.* **14**(3), 280–284 (2015).

43. E. Zhang et al., "Magnetotransport properties of Cd₃As₂ nano-structures," *ACS Nano* **9**(9), 8843–8850 (2015).

44. C. Li et al., "Synthesis and photovoltaic properties of Cd₃As₂ faceted nanoplates and nano-octahedrons," *Cryst. Growth Design* **15**(7), 3264–3270 (2015).

45. M. Uchida et al., "Quantum hall states observed in thin films of Dirac semimetal Cd₃As₂," *Nat. Commun.* **8**, 2274 (2017).

46. M. Yang et al., "Ultraviolet to long-wave infrared photodetectors based on a three-dimensional Dirac semimetal/organic thin film heterojunction," *J. Phys. Chem. Lett.* **10**(14), 3914–3921 (2019).

47. K. Zhang et al., "Controllable synthesis and magnetotransport properties of Cd₃As₂ Dirac semimetal nanostructures," *RSC Adv.* **7**(29), 17689–17696 (2017).

48. W. Zhuang, Z. Chen, and X. Wang, "Large-area fabrication of 2D layered topological semimetal films and emerging applications," *Adv. Phys. X* **7**(1), 2034529 (2022).

49. T. Schumann et al., "Observation of the quantum hall effect in confined films of the three-dimensional Dirac semimetal Cd₃As₂," *Phys. Rev. Lett.* **120**(1), 16801 (2018).

50. Y. Yan et al., "Modify Cd₃As₂ nanowires with sulfur to fabricate self-powered NIR photodetectors with enhanced performance," *Nano Res.* **14**(10), 3379–3385 (2021).

51. J. J. Dubowski and D. F. Williams, "Growth of polycrystalline Cd₃As₂ films on room temperature substrates by a pulsed-laser evaporation technique," *Thin Solid Films* **117**(4), 289–297 (1984).

52. Y. F. Wu et al., "Dirac semimetal heterostructures: 3D Cd₃As₂ on 2D graphene," *Adv. Mater.* **30**(34), 1707547 (2018).

53. R. Sankar et al., "Large single crystal growth, transport property, and spectroscopic characterizations of three-dimensional Dirac semimetal Cd₃As₂," *Sci. Rep.* **5**, 12966 (2015).

54. H.-U. Krebs et al., "Pulsed laser deposition (PLD)—a versatile thin film technique," *Adv. Solid State Phys.* **43**, 505–518 (2003).

55. J. Schou, "Physical aspects of the pulsed laser deposition technique: the stoichiometric transfer of material from target to film," *Appl. Surf. Sci.* **255**(10), 5191–5198 (2009).

56. S. M. Rossnagel, "Thin film deposition with physical vapor deposition and related technologies," *J. Vac. Sci. Technol. A Vac. Surf. Film* **21**(5), S74–S87 (2003).

57. X. Zhang et al., "High-performance photodetector based on a 3D Dirac semimetal Cd 3 As 2 /Tungsten disulfide (WS 2) van Der Waals heterojunction," *Adv. Photonics Res.* **2**(6), 2000194 (2021).

58. Z. G. Chen et al., "Scalable growth of high mobility Dirac semimetal Cd₃As₂ microbelts," *Nano Lett.* **15**(9), 5830–5834 (2015).

59. A. Szczerbakow and K. Durose, "Self-selecting vapour growth of bulk crystals—principles and applicability," *Progr. Cryst. Growth Charact. Mater.* **51**(1–3), 81–108 (2005).

60. M. Goyal et al., "Thickness dependence of the quantum hall effect in films of the three-dimensional Dirac semimetal Cd₃As₂," *APL Mater.* **6**(2), 026105 (2018).

61. G. Liang et al., "Strain-induced circular photogalvanic current in Dirac semimetal Cd₃As₂ films epitaxied on a GaAs(111)B substrate," *Nanoscale* **14**(6), 2383–2392 (2022).

62. Y. Miyazaki et al., "Quantum oscillations from Fermi arc surface states in Cd₃As₂ submicron wires," *Phys. Rev. Res.* **4**(2), L022002 (2022).

63. W. Yu et al., "Evidence of decoupling of surface and bulk states in Dirac semimetal Cd₃As₂," *Nanotechnology* **33**(41), 415002 (2022).

64. T. Schumann et al., "Observation of the quantum hall effect in confined films of the three-dimensional Dirac semimetal Cd₃As₂," *Phys. Rev. Lett.* **120**(1), 016801 (2018).

65. S. N. Ogugua, O. M. Ntwaeaborwa, and H. C. Swart, "Latest development on pulsed laser deposited thin films for advanced luminescence applications," *Coatings* **10**(11), 1–22 (2020).

66. L. M. Kukreja et al., "Pulsed laser deposition of plasmonic-metal nanostructures," *J. Phys. D. Appl. Phys.* **47**(3), 034015 (2014).

67. Y. Bleu et al., "Review of graphene growth from a solid carbon source by pulsed laser deposition (PLD)," *Front. Chem.* **6**, 572 (2018).

68. K. Q. Lin, S. Bange, and J. M. Lupton, "Quantum interference in second-harmonic generation from monolayer WSe₂," *Nat. Phys.* **15**(3), 242–246 (2019).

69. R. Zhou et al., "Engineering the harmonic generation in graphene," *Mater. Today Phys.* **23**, 100649 (2022).

70. J. Zhang et al., "Second harmonic generation in 2D layered materials," *2D Mater.* **7**(4), 042002 (2020).

71. Y. Wang et al., "Second harmonic generation spectroscopy on two-dimensional materials [invited]," *Opt. Mater. Express* **9**(3), 1136 (2019)

72. L. Bonacina et al., "Harmonic generation at the nanoscale," *J. Appl. Phys.* **127**(23), 230901 (2020).

73. H. Ma et al., "Rich information on 2D materials revealed by optical second harmonic generation," *Nanoscale* **12**(45), 22891–22903 (2020).

74. A. Autere et al., "Nonlinear optics with 2D layered materials," *Adv. Mater.* **30**(24), 1705963 (2018).

75. X. Wen, Z. Gong, and D. Li, "Nonlinear optics of two-dimensional transition metal dichalcogenides," *InfoMat* **1**(3), 317–337 (2019).

76. H. A. Atwater and A. Polman, "Plasmonics for improved photovoltaic devices," *Nat. Mater.* **9**(3), 205–213 (2010).

77. G. Baffou and R. Quidant, "Thermo-plasmonics: using metallic nanostructures as nano-sources of heat," *Laser Photonics Rev.* **7**(2), 171–187 (2013).

78. N. C. Panoiu et al., "Nonlinear optics in plasmonic nanostructures," *J. Opt.* **20**(8), 083001 (2018).

79. D. Marinica et al., "Quantum plasmonics: nonlinear effects in the field enhancement of a plasmonic nanoparticle Dimer," *Nano Lett.* **12**(3), 1333–1339 (2012).

80. S. Bidault, M. Mivelle, and N. Bonod, "Dielectric nanoantennas to manipulate solid-state light emission," *J. Appl. Phys.* **126**(9), 094104 (2019).

81. K. Ullah et al., "Engineering the optical properties of dielectric nanospheres by resonant modes," *Nanotechnology* **29**(50), 505204 (2018).

82. M. Decker et al., "High-efficiency dielectric Huygens' surfaces," *Adv. Opt. Mater.* **3**(6), 813–820 (2015).

83. K. S. Novoselov et al., "Electric field in atomically thin carbon films," *Science* **306**(5696), 666–669 (2004).

84. R. Ma, D. S. Sutherland, and Y. Shi, "Harmonic generation in transition metal dichalcogenides and their heterostructures," *Mater. Today* **50**, 570–586 (2021).

85. R. A. Ganeev et al., "Characterization of nonlinear optical parameters of KDP, LiNbO₃ and BBO crystals," *Opt. Commun.* **229**(1–6), 403–412 (2004).

86. P. Bharadwaj, B. Deutsch, and L. Novotny, "Optical antennas," *Adv. Opt. Photonics* **1**(3), 438 (2009).

87. P. Y. Chen et al., "Enhanced nonlinearities using plasmonic nano-antennas," *Nanophotonics* **1**(3–4), 221–233 (2012).

88. R. W. Boyd, Z. Shi, and I. De Leon, "The third-order nonlinear optical susceptibility of gold," *Opt. Commun.* **326**, 74–79 (2014).

89. J. Renger, R. Quidant, and L. Novotny, "Enhanced nonlinear response from metal surfaces," *Opt. Express* **19**(3), 1777 (2011).

90. R. W. Boyd, *Nonlinear Optics*, 4th ed., Academic Press, Oxford, United Kingdom (2020).

91. K. Ullah et al., "Harmonic generation in low-dimensional materials," *Adv. Opt. Mater.* **10**(7), 2101860 (2022).

92. A. Autere et al., "Nonlinear optics with 2D layered materials," *Adv. Mater.* **30**(24), 1–24 (2018).

93. K. Ullah et al., "Third harmonic generation in Dirac semimetal Cd₃As₂," *Appl. Phys. Lett.* **117**(1), 011102 (2020)

94. J. Lim et al., "Efficient generation of extreme terahertz harmonics in three-dimensional Dirac semimetals," *Phys. Rev. Res.* **2**(4), 043252 (2020).

95. B. Cheng et al., "Efficient terahertz harmonic generation with coherent acceleration of electrons in the Dirac semimetal Cd₃As₂," *Phys. Rev. Lett.* **124**(11), 117402 (2020).

96. T. Zhang et al., "Optical Kerr effect and third harmonic generation in topological Dirac/Weyl semimetal," *Opt. Express* **27**(26), 38270 (2019).

97. Y. Gao and B. Ge, "Second harmonic generation in Dirac/Weyl semimetals with broken tilt inversion symmetry," *Opt. Express* **29**(5), 6903 (2021).

98. L. Ju et al., "Graphene plasmonics for tunable terahertz metamaterials," *Nat. Nanotechnol.* **6**(10), 630–634 (2011).

99. H. Yan et al., "Tunable infrared plasmonic devices using graphene/insulator stacks," *Nat. Nanotechnol.* **7**(5), 330–334 (2012).

100. A. Chanana et al., "Manifestation of kinetic inductance in terahertz Plasmon resonances in thin-film Cd₃As₂," *ACS Nano* **13**(4), 4091–4100 (2019).

101. S. Das Sarma and Q. Li, "Intrinsic plasmons in two-dimensional Dirac materials," *Phys. Rev. B - Condens. Matter Mater. Phys.* **87**(23), 235418 (2013).

102. T. Low and P. Avouris, "Graphene plasmonics for terahertz to mid-infrared applications," *ACS Nano* **8**(2), 1086–1101 (2014).

103. J. Hofmann and S. Das Sarma, "Plasmon signature in Dirac-Weyl liquids," *Phys. Rev. B - Condens. Matter Mater. Phys.* **91**(24), 241108 (2015).

104. D. E. Kharzeev, R. D. Pisarski, and H. U. Yee, "Universality of plasmon excitations in Dirac semimetals," *Phys. Rev. Lett.* **115**(23), 236402 (2015).

105. H. Chen et al., "Realization of tunable plasmon-induced transparency by bright-bright mode coupling in Dirac semimetals," *Opt. Mater. Express* **7**(9), 3397 (2017).

106. X. He et al., "Tunable 3D Dirac-semimetals supported mid-IR hybrid plasmonic waveguides," *Opt. Lett.* **46**(3), 472 (2021).

107. Y. Su et al., "Controlling terahertz surface plasmon polaritons in Dirac semimetal sheets," *Opt. Mater. Express* **8**(4), 884 (2018).

108. X. He et al., "Tunable terahertz Dirac-semimetal hybrid plasmonic waveguides," *Opt. Mater. Express* **12**(1), 73 (2022).

109. Z. Lu and W. Zhao, "Nanoscale electro-optic modulators based on graphene-slot waveguides," *J. Opt. Soc. Am. B* **29**(6), 1490 (2012).

110. S. A. Mikhailov and K. Ziegler, "New electromagnetic mode in graphene," *Phys. Rev. Lett.* **99**(1), 016803 (2007).

111. M. Bordag and I. G. Pirozhenko, "Transverse-electric surface plasmon for graphene in the Dirac equation model," *Phys. Rev. B - Condens. Matter Mater. Phys.* **89**(3), 035421 (2014).

112. S. Roy and P. C. Subramaniam, "TE-polarized surface plasmon Polaritons in metal waveguides bounded by self-focusing and self-defocusing media," *Opt. Lett.* **17**(13), 911 (1992).

113. W. Zhang et al., "Ultrafast photocarrier dynamics in a 3D Dirac semimetal Cd₃As₂ film studied with terahertz spectroscopy," *Appl. Phys. Lett.* **114**(22), 221102 (2019).

114. X. Y. He, J. Tao, and B. Meng, "Analysis of graphene TE surface plasmons in the terahertz regime," *Nanotechnology* **24**(34), 345203 (2013).

115. M. Jablan, H. Buljan, and M. Soljačić, "Transverse electric plasmons in bilayer graphene," *Opt. Express* **19**(12), 11236 (2011).

116. M. Y. Musa et al., "Confined transverse electric phonon polaritons in hexagonal Boron Nitrides," *2D Mater.* **5**(1), 015018 (2018).

117. D. Drosdoff, A. D. Phan, and L. M. Woods, "Transverse electric mode for near-field radiative heat transfer in graphene-metamaterial systems," *Adv. Opt. Mater.* **2**(11), 1038–1042 (2014).

118. Y. V. Bludov et al., "Nonlinear TE-polarized surface polaritons on graphene," *Phys. Rev. B - Condens. Matter Mater. Phys.* **89**(3), 035406 (2014).

119. H. Xiong and Q. A. Shen, "Thermally and electrically dual-tunable absorber based on Dirac semimetal and strontium titanate," *Nanoscale* **12**(27), 14598–14604 (2020).

120. H. Xiong, D. Li, and H. Zhang, "Broadband terahertz absorber based on hybrid Dirac semimetal and water," *Opt. Laser Technol.* **143**, 107274 (2021).

121. H. Xiong et al., "Bi-tunable terahertz absorber based on strontium titanate and Dirac semimetal," *Opt. Express* **28**(10), 15744 (2020).

122. X. He et al., "3D Dirac semimetal supported tunable TE modes," *Ann. Phys.* **534**(4), 1–8 (2022).

123. R. D. Kekatpure et al., "Phase-coupled plasmon-induced transparency," *Phys. Rev. Lett.* **104**(24), 243902 (2010).

124. S. Zhang et al., "Plasmon-induced transparency in metamaterials," *Phys. Rev. Lett.* **101**(4), 047401 (2008).

125. J. T. Liu and Z. Liu, "Robust tunable plasmon induced transparency in coupled-resonance finite array of metasurface nanostructure," *Sci. Rep.* **11**, 1221 (2021).

126. S. Paul and M. Ray, "Multispectral switching using Fano resonance and plasmon-induced transparency in a plasmonic waveguide-coupled resonator system," *Plasmonics* **14**(5), 1113–1122 (2019).

127. Z. Li et al., "Manipulating the plasmon-induced transparency in terahertz metamaterials," *Opt. Express* **19**(9), 8912 (2011).

128. S. Yang et al., "Enhanced second-order nonlinearity and tunable plasmon induced transparency in noncoplanar Dirac semimetal system," *Solid State Commun.* **340**(February), 114510 (2021).

129. H. Chen et al., "Tunable multiple plasmon-induced transparency in three-dimensional Dirac semimetal metamaterials," *Opt. Commun.* **423**, 57–62 (2018).

130. H. Chen et al., "Broadband tunable terahertz plasmon-induced transparency in Dirac semimetals," *Opt. Laser Technol.* **104**, 210–215 (2018).

131. Y. Li, X. Zhai, and L. Wang, "Dynamically tunable plasmon-induced absorption in Dirac semimetal waveguide," *Opt. Commun.* **437**(2018), 246–250 (2019).

132. C. P. Weber, "Ultrafast investigation and control of Dirac and Weyl semimetals," *J. Appl. Phys.* **129**(7), 070901.

133. C. P. Weber et al., "Similar ultrafast dynamics of several dissimilar Dirac and Weyl semimetals," *J. Appl. Phys.* **122**(22), 223102 (2017).

134. C. Zhu et al., "A robust and tuneable mid-infrared optical switch enabled by bulk Dirac fermions," *Nat. Commun.* **8**, 14111 (2017).

135. J. Liu et al., "Semimetals for high-performance photodetection," *Nat. Mater.* **19**(8), 830–837 (2020).

136. C. P. Weber et al., "Transient reflectance of photoexcited Cd₃As₂," *Appl. Phys. Lett.* **106**(23), 1–5 (2015).

137. C. Zhu et al., "Broadband hot-carrier dynamics in three-dimensional Dirac semimetal Cd₃As₂," *Appl. Phys. Lett.* **111**(9), 2–6 (2017).

138. W. Lu et al., "Ultrafast relaxation dynamics of photoexcited Dirac fermions in the three-dimensional Dirac semimetal Cd₃As₂," *Phys. Rev. B* **95**(2), 024303 (2017).

139. W. Lu et al., "Terahertz probe of photoexcited carrier dynamics in the Dirac semimetal Cd₃As₂," *Phys. Rev. B* **98**(10), 104310 (2018).

140. N. Landy et al., "Perfect metamaterial absorber," *Phys. Rev. Lett.* **100**(20), 207402 (2008).

141. B. Wang et al., "A novel ultrathin and broadband microwave metamaterial absorber," *J. Appl. Phys.* **116**(9), 094504 (2014).

142. H. Tao et al., "Highly flexible wide angle of incidence terahertz metamaterial absorber: design, fabrication, and characterization," *Phys. Rev. B - Condens. Matter Mater. Phys.* **78**(24), 241103 (2008).

143. J. Xu et al., "Design of triple-band metamaterial absorbers with refractive index sensitivity at infrared frequencies," *Opt. Express* **24**(22), 25742 (2016).

144. X. Lu, L. Zhang, and T. Zhang, "Nanoslit-microcavity-based narrow band absorber for sensing applications," *Opt. Express* **23**(16), 20715 (2015).

145. N. Liu et al., "Infrared perfect absorber and its application as plasmonic sensor," *Nano Lett.* **10**(7), 2342–2348 (2010).

146. G. Li et al., "Novel plasmonic resonance sensor based on an infra-red perfect absorber," *J. Phys. D. Appl. Phys.* **45**(20), 205102 (2012).

147. J. He et al., "Ultra-narrow band perfect absorbers based on plasmonic analog of electromagnetically induced absorption," *Opt. Express* **23**(5), 6083 (2015).

148. Y. Qu et al., "Spatially and spectrally resolved narrowband optical absorber based on 2D grating nanostructures on metallic films," *Adv. Opt. Mater.* **4**(3), 480–486 (2016).

149. Y. Gong et al., "Coherent emission of light using stacked gratings," *Phys. Rev. B - Condens. Matter Mater. Phys.* **87**(20), 205121 (2013).

150. X. Liu et al., "Taming the blackbody with infrared metamaterials as selective thermal emitters," *Phys. Rev. Lett.* **107**(4), 045901 (2011).

151. Z. Song and B. Zhang, "Wide-angle polarization-insensitive transparency of a continuous opaque metal film for near-infrared light," *Opt. Express* **22**(6), 6519 (2014).

152. S. Fan and J. D. Joannopoulos, "Analysis of guided resonances in photonic crystal slabs," *Phys. Rev. B - Condens. Matter Mater. Phys.* **65**(23), 235112 (2002).

153. G. D. Liu et al., "A high-performance refractive index sensor based on Fano resonance in Si split-ring metasurface," *Plasmonics* **13**(1), 15–19 (2018).

154. M. Chen et al., "Dynamically tunable polarization-independent terahertz absorber based on bulk Dirac semimetals," *OSA Contin.* **2**(8), 2477 (2019).

155. H. Lin et al., "Graphene multilayer photonic metamaterials: fundamentals and applications," *Adv. Mater. Technol.* **6**(5), 1–26 (2021).

156. G.-D. Liu et al., "Dirac semimetals based tunable narrowband absorber at terahertz frequencies," *Opt. Express* **26**(9), 11471 (2018).

157. L. Dai et al., "Dynamically tunable broadband linear-to-circular polarization converter based on Dirac semimetals," *Opt. Mater. Express* **8**(10), 3238 (2018).

158. Z. Wang et al., "Ultrahigh-Q tunable terahertz absorber based on bulk Dirac semimetal with surface lattice resonance," *Photonics* **9**(1), 22 (2022).

159. J. Wang, X. Wan, and Y. Jiang, "Tunable triple-band terahertz absorber based on bulk-Dirac-semimetal metasurface," *IEEE Photonics J.* **13**(4), 1–5 (2021).

160. H. Liu and P. Lalanne, "Microscopic theory of the extraordinary optical transmission," *Nature* **452**(7188), 728–731 (2008).

161. F. Wu et al., "Control on surface plasmon polaritons propagation properties by continuously moving a nanoparticle along a silver nanowire waveguide," *Sci. Rep.* **6**, 37512 (2016).

162. L. M. Wang et al., "Dynamics of coupled plasmon polariton wave packets excited at a subwavelength slit in optically thin metal films," *Phys. Rev. B - Condens. Matter Mater. Phys.* **86**(16), 165408 (2012).

163. F. Van Beijnum et al., "Quasi-cylindrical wave contribution in experiments on extraordinary optical transmission," *Nature* **492**(7429), 411–414 (2012).

164. Z. Xue et al., "Ultraviolet/visible quasicylindrical waves on semimetal Cd₃As₂ nanoplates," *Adv. Photonics Res.* **3**(4), 2100354 (2022).

165. J. Huang et al., "Switchable coding metasurface for flexible manipulation of terahertz wave based on Dirac semimetal," *Results Phys.* **33**, 105204 (2022).

166. C. Della Giovampaola and N. Engheta, "Digital metamaterials," *Nat. Mater.* **13**(12), 1115–1121 (2014).

167. T. J. Cui, S. Liu, and L. Zhang, "Information metamaterials and metasurfaces," *J. Mater. Chem. C* **5**(15), 3644–3668 (2017).

168. T. J. Cui et al., "Coding Metamaterials, digital metamaterials and programmable metamaterials," *Light Sci. Appl.* **3**(10), e218–e218 (2014).

169. C. Zhou et al., "Graphene-embedded coding metasurface for dynamic terahertz manipulation," *Optik* **216**, 164937 (2020).

170. Y. M. Qing, H. F. Ma, and T. J. Cui, "Multifunctional space-time-coding amplitude modulated graphene metasurfaces," *J. Opt. Soc. Am. B* **38**(10), 3206 (2021).

171. J. Ma et al., "Experimental progress on layered topological semimetals," *2D Mater.* **6**(3), 032001 (2019).

172. C. Zhang et al., "Room-temperature chiral charge pumping in Dirac semimetals," *Nat. Commun.* **8**, 13741 (2017).

173. U. Keller, "Recent developments in compact ultrafast lasers," *Nature* **424**, 831–838 (2003).

174. U. Keller et al., "Solid-state low-loss intracavity saturable absorber for Nd:YLF lasers: an antiresonant semiconductor Fabry–Perot saturable absorber," *Opt. Lett.* **17** (7), 505–507 (1992).

175. U. Keller et al., "Semiconductor saturable absorber mirrors (SESAM's) for femtosecond to nanosecond pulse generation in solid-state lasers," *IEEE J. Sel. Top. Quantum Electron.* **2**(3), 435–453 (1996).

176. Y. Yang and F. Xiu, "Broadband photodetection of Cd₃As₂: review and perspectives," *Mater. Today Electron.* **2**(July), 100007 (2022).

177. X. Zhang et al., "3D Dirac semimetal Cd₃As₂/CuPc heterojunction for promoted visible-infrared photo-detection," *Opt. Mater.* **111**(2020), 110699 (2021).

178. C. Liu et al., "A review of graphene plasmons and its combination with metasurface," *J. Korean Ceram. Soc.* **54**(5), 349–365 (2017).

179. M. Yang et al., "Enhanced performance of wideband room temperature photodetector based on Cd₃As₂ thin film/pentacene heterojunction," *ACS Photonics* **5**(8), 3438–3445 (2018).

Renlong Zhou received his BS degree from Hunan University of Science and Technology (HNUST) in 1998, his MS degree from Hunan University (HNU) in 2003, and his PhD from Shanghai Institute of Technical Physics (SITP) of the Chinese Academy of Sciences (CAS) in 2007. Currently, he is a professor at the School of Physics and Information Engineering, Guangdong University of Education, Guangzhou, China. He directs the Research Institute of Terahertz Functional Devices. His research interests include photonic crystals, two-dimensional materials, light–matter interaction, nonlinear optics, surface plasmon, and applications.

Kaleem Ullah received his PhD in optical engineering from Nanjing University of Science and Technology (NJUST), China, in 2018. After that, he completed his postdoctoral fellowship at Nanjing University, China. Currently, he is a postdoctoral researcher at the University of Delaware, United States. His research interests include far-field super resolution microscopy, nanophotonics of dielectric nanostructures, plasmonics, integrated photonics, and light–matter interaction in two-dimensional materials.

Naveed Hussain received his master's degree in physics from International Islamic University, Islamabad, Pakistan, in 2012, and his PhD from the School of Materials, Tsinghua university, Beijing, China, in 2019. Currently, he is working as a senior postdoctoral researcher at the School of Electrical and Computer Engineering, University of California Irvine. His research focuses on high-pressure syntheses and crystallographic engineering of ultrathin two-dimensiona materials, probed by using light–matter interactions at the nanoscale.

Mohammed M. Fadhali received his BSc degree from the University of Technology, Iraq, in 1997, his MSc degree from Cochin University of Science and Technology, India, in 2003, and his PhD from Universiti Teknologi Malaysia, in 2008. Currently, he is an associate professor of laser physics/photonics at Physics Department, Jazan University, Saudi Arabia. His research interests include ultrafast optical process, laser spectroscopy, plasmonic, and nanophotonic.

Sa Yang received her BE degree from Chengdu University of Information Technology (CUIT) in 1992 and her ME degree from South China

University of Technology (SCUT) in 2007. He is an associate professor at the School of Physics and Information Engineering, Guangdong University of Education, Guangzhou, China. She is the dean of the School of Physical and Information Engineering. Her research interests include optoelectronic device design, micro/nano material characteristic analysis, and image information processing.

Qiawu Lin received his BS degree from Guangdong University of Education, China, in 2003, and his MS degree from Sun Yat-sen University, China, in 2010. Currently, he is pursuing a PhD at South China Normal University, China. Currently, he is an associate professor in the Department of Physics and Information Engineering, Guangdong University of Education, Guangzhou, China. He is the assistant dean of the Department of Physics and Information Engineering. His research interests include photonic crystals, two-dimensional materials, nonlinear optics, surface plasmon, and applications.

Muhammad Zubair received his PhD from Beijing University of Technology, China, in 2020. Currently, he is working as a research scientist in the Forschungszentrum Jülich, and will focus on the development of cathodes and electrolytes of solid-state lithium metal batteries. His research interests lie in synthesis and characterization of cathode materials for batteries.

Muhammad Faisal Iqbal received his PhD in physics from the University of Science and Technology of China, Hefei, China, in 2020. Currently, he is working as an assistant professor in the Department of Physics, Riphah International University Faisalabad, Pakistan. His current research interests are mainly focused on Raman spectroscopy, surface-enhanced Raman spectroscopy, and optoelectronic properties of semiconductor thin films and nanostructures.